PHYSICAL REVIEW D **76,** 052005 (2007)

Measurement of the hadronic form factor in $D^0 \to K^- e^+ \nu_e$ decays

B. Aubert,[1] M. Bona,[1] D. Boutigny,[1] Y. Karyotakis,[1] J. P. Lees,[1] V. Poireau,[1] X. Prudent,[1] V. Tisserand,[1] A. Zghiche,[1] J. Garra Tico,[2] E. Grauges,[2] L. Lopez,[3] A. Palano,[3] G. Eigen,[4] B. Stugu,[4] L. Sun,[4] G. S. Abrams,[5] M. Battaglia,[5] D. N. Brown,[5] J. Button-Shafer,[5] R. N. Cahn,[5] Y. Groysman,[5] R. G. Jacobsen,[5] J. A. Kadyk,[5] L. T. Kerth,[5] Yu. G. Kolomensky,[5] G. Kukartsev,[5] D. Lopes Pegna,[5] G. Lynch,[5] L. M. Mir,[5] T. J. Orimoto,[5] M. T. Ronan,[5,*] K. Tackmann,[5] W. A. Wenzel,[5] P. del Amo Sanchez,[6] C. M. Hawkes,[6] A. T. Watson,[6] T. Held,[7] H. Koch,[7] B. Lewandowski,[7] M. Pelizaeus,[7] T. Schroeder,[7] M. Steinke,[7] D. Walker,[8] D. J. Asgeirsson,[9] T. Cuhadar-Donszelmann,[9] B. G. Fulsom,[9] C. Hearty,[9] N. S. Knecht,[9] T. S. Mattison,[9] J. A. McKenna,[9] A. Khan,[10] M. Saleem,[10] L. Teodorescu,[10] V. E. Blinov,[11] A. D. Bukin,[11] V. P. Druzhinin,[11] V. B. Golubev,[11] A. P. Onuchin,[11] S. I. Serednyakov,[11] Yu. I. Skovpen,[11] E. P. Solodov,[11] K. Yu Todyshev,[11] M. Bondioli,[12] S. Curry,[12] I. Eschrich,[12] D. Kirkby,[12] A. J. Lankford,[12] P. Lund,[12] M. Mandelkern,[12] E. C. Martin,[12] D. P. Stoker,[12] S. Abachi,[13] C. Buchanan,[13] S. D. Foulkes,[14] J. W. Gary,[14] F. Liu,[14] O. Long,[14] B. C. Shen,[14] L. Zhang,[14] H. P. Paar,[15] S. Rahatlou,[15] V. Sharma,[15] J. W. Berryhill,[16] C. Campagnari,[16] A. Cunha,[16] B. Dahmes,[16] T. M. Hong,[16] D. Kovalskyi,[16] J. D. Richman,[16] T. W. Beck,[17] A. M. Eisner,[17] C. J. Flacco,[17] C. A. Heusch,[17] J. Kroseberg,[17] W. S. Lockman,[17] T. Schalk,[17] B. A. Schumm,[17] A. Seiden,[17] D. C. Williams,[17] M. G. Wilson,[17] L. O. Winstrom,[17] E. Chen,[18] C. H. Cheng,[18] F. Fang,[18] D. G. Hitlin,[18] I. Narsky,[18] T. Piatenko,[18] F. C. Porter,[18] G. Mancinelli,[19] B. T. Meadows,[19] K. Mishra,[19] M. D. Sokoloff,[19] F. Blanc,[20] P. C. Bloom,[20] S. Chen,[20] W. T. Ford,[20] J. F. Hirschauer,[20] A. Kreisel,[20] M. Nagel,[20] U. Nauenberg,[20] A. Olivas,[20] J. G. Smith,[20] K. A. Ulmer,[20] S. R. Wagner,[20] J. Zhang,[20] A. M. Gabareen,[21] A. Soffer,[21] W. H. Toki,[21] R. J. Wilson,[21] F. Winklmeier,[21] Q. Zeng,[21] D. D. Altenburg,[22] E. Feltresi,[22] A. Hauke,[22] H. Jasper,[22] J. Merkel,[22] A. Petzold,[22] B. Spaan,[22] K. Wacker,[22] T. Brandt,[23] V. Klose,[23] M. J. Kobel,[23] H. M. Lacker,[23] W. F. Mader,[23] R. Nogowski,[23] J. Schubert,[23] K. R. Schubert,[23] R. Schwierz,[23] J. E. Sundermann,[23] A. Volk,[23] D. Bernard,[24] G. R. Bonneaud,[24] E. Latour,[24] V. Lombardo,[24] Ch. Thiebaux,[24] M. Verderi,[24] P. J. Clark,[25] W. Gradl,[25] F. Muheim,[25] S. Playfer,[25] A. I. Robertson,[25] Y. Xie,[25] M. Andreotti,[26] D. Bettoni,[26] C. Bozzi,[26] R. Calabrese,[26] A. Cecchi,[26] G. Cibinetto,[26] P. Franchini,[26] E. Luppi,[26] M. Negrini,[26] A. Petrella,[26] L. Piemontese,[26] E. Prencipe,[26] V. Santoro,[26] F. Anulli,[27] R. Baldini-Ferroli,[27] A. Calcaterra,[27] R. de Sangro,[27] G. Finocchiaro,[27] S. Pacetti,[27] P. Patteri,[27] I. M. Peruzzi,[27,†] M. Piccolo,[27] M. Rama,[27] A. Zallo,[27] A. Buzzo,[28] R. Contri,[28] M. Lo Vetere,[28] M. M. Macri,[28] M. R. Monge,[28] S. Passaggio,[28] C. Patrignani,[28] E. Robutti,[28] A. Santroni,[28] S. Tosi,[28] K. S. Chaisanguanthum,[29] M. Morii,[29] J. Wu,[29] R. S. Dubitzky,[30] J. Marks,[30] S. Schenk,[30] U. Uwer,[30] D. J. Bard,[31] P. D. Dauncey,[31] R. L. Flack,[31] J. A. Nash,[31] M. B. Nikolich,[31] W. Panduro Vazquez,[31] P. K. Behera,[32] X. Chai,[32] M. J. Charles,[32] U. Mallik,[32] N. T. Meyer,[32] V. Ziegler,[32] J. Cochran,[33] H. B. Crawley,[33] L. Dong,[33] V. Eyges,[33] W. T. Meyer,[33] S. Prell,[33] E. I. Rosenberg,[33] A. E. Rubin,[33] A. V. Gritsan,[34] Z. J. Guo,[34] C. K. Lae,[34] A. G. Denig,[35] M. Fritsch,[35] G. Schott,[35] N. Arnaud,[36] J. Béquilleux,[36] M. Davier,[36] G. Grosdidier,[36] A. Höcker,[36] V. Lepeltier,[36] F. Le Diberder,[36] A. M. Lutz,[36] S. Pruvot,[36] S. Rodier,[36] P. Roudeau,[36] M. H. Schune,[36] J. Serrano,[36] V. Sordini,[36] A. Stocchi,[36] W. F. Wang,[36] G. Wormser,[36] D. J. Lange,[37] D. M. Wright,[37] C. A. Chavez,[38] I. J. Forster,[38] J. R. Fry,[38] E. Gabathuler,[38] R. Gamet,[38] D. E. Hutchcroft,[38] D. J. Payne,[38] K. C. Schofield,[38] C. Touramanis,[38] A. J. Bevan,[39] K. A. George,[39] F. Di Lodovico,[39] W. Menges,[39] R. Sacco,[39] G. Cowan,[40] H. U. Flaecher,[40] D. A. Hopkins,[40] P. S. Jackson,[40] T. R. McMahon,[40] F. Salvatore,[40] A. C. Wren,[40] D. N. Brown,[41] C. L. Davis,[41] J. Allison,[42] N. R. Barlow,[42] R. J. Barlow,[42] Y. M. Chia,[42] C. L. Edgar,[42] G. D. Lafferty,[42] T. J. West,[42] J. I. Yi,[42] J. Anderson,[43] C. Chen,[43] A. Jawahery,[43] D. A. Roberts,[43] G. Simi,[43] J. M. Tuggle,[43] G. Blaylock,[44] C. Dallapiccola,[44] S. S. Hertzbach,[44] X. Li,[44] T. B. Moore,[44] E. Salvati,[44] S. Saremi,[44] R. Cowan,[45] P. H. Fisher,[45] G. Sciolla,[45] S. J. Sekula,[45] M. Spitznagel,[45] F. Taylor,[45] R. K. Yamamoto,[45] S. E. Mclachlin,[46] P. M. Patel,[46] S. H. Robertson,[46] A. Lazzaro,[47] F. Palombo,[47] J. M. Bauer,[48] L. Cremaldi,[48] V. Eschenburg,[48] R. Godang,[48] R. Kroeger,[48] D. A. Sanders,[48] D. J. Summers,[48] H. W. Zhao,[48] S. Brunet,[49] D. Côté,[49] M. Simard,[49] P. Taras,[49] F. B. Viaud,[49] H. Nicholson,[50] G. De Nardo,[51] F. Fabozzi,[51,‡] L. Lista,[51] D. Monorchio,[51] C. Sciacca,[51] M. A. Baak,[52] G. Raven,[52] H. L. Snoek,[52] C. P. Jessop,[53] J. M. LoSecco,[53] G. Benelli,[54] L. A. Corwin,[54] K. K. Gan,[54] K. Honscheid,[54] D. Hufnagel,[54] H. Kagan,[54] R. Kass,[54] J. P. Morris,[54] A. M. Rahimi,[54] J. J. Regensburger,[54] R. Ter-Antonyan,[54] Q. K. Wong,[54] N. L. Blount,[55] J. Brau,[55] R. Frey,[55] O. Igonkina,[55] J. A. Kolb,[55] M. Lu,[55] R. Rahmat,[55] N. B. Sinev,[55] D. Strom,[55] J. Strube,[55] E. Torrence,[55] N. Gagliardi,[56] A. Gaz,[56] M. Margoni,[56] M. Morandin,[56] A. Pompili,[56] M. Posocco,[56] M. Rotondo,[56] F. Simonetto,[56] R. Stroili,[56] C. Voci,[56] E. Ben-Haim,[57] H. Briand,[57] G. Calderini,[57] J. Chauveau,[57] P. David,[57] L. Del Buono,[57] Ch. de la Vaissière,[57] O. Hamon,[57] Ph. Leruste,[57] J. Malclès,[57] J. Ocariz,[57] A. Perez,[57] L. Gladney,[58] M. Biasini,[59] R. Covarelli,[59] E. Manoni,[59] C. Angelini,[60] G. Batignani,[60] S. Bettarini,[60] M. Carpinelli,[60] R. Cenci,[60] A. Cervelli,[60] F. Forti,[60] M. A. Giorgi,[60] A. Lusiani,[60]

G. Marchiori,[60] M. A. Mazur,[60] M. Morganti,[60] N. Neri,[60] E. Paoloni,[60] G. Rizzo,[60] J. J. Walsh,[60] M. Haire,[61] J. Biesiada,[62] P. Elmer,[62] Y. P. Lau,[62] C. Lu,[62] J. Olsen,[62] A. J. S. Smith,[62] A. V. Telnov,[62] E. Baracchini,[63] F. Bellini,[63] G. Cavoto,[63] A. D'Orazio,[63] D. del Re,[63] E. Di Marco,[63] R. Faccini,[63] F. Ferrarotto,[63] F. Ferroni,[63] M. Gaspero,[63] P. D. Jackson,[63] L. Li Gioi,[63] M. A. Mazzoni,[63] S. Morganti,[63] G. Piredda,[63] F. Polci,[63] F. Renga,[63] C. Voena,[63] M. Ebert,[64] H. Schröder,[64] R. Waldi,[64] T. Adye,[65] G. Castelli,[65] B. Franek,[65] E. O. Olaiya,[65] S. Ricciardi,[65] W. Roethel,[65] F. F. Wilson,[65] R. Aleksan,[66] S. Emery,[66] M. Escalier,[66] A. Gaidot,[66] S. F. Ganzhur,[66] G. Hamel de Monchenault,[66] W. Kozanecki,[66] M. Legendre,[66] G. Vasseur,[66] Ch. Yèche,[66] M. Zito,[66] X. R. Chen,[67] H. Liu,[67] W. Park,[67] M. V. Purohit,[67] J. R. Wilson,[67] M. T. Allen,[68] D. Aston,[68] R. Bartoldus,[68] P. Bechtle,[68] N. Berger,[68] R. Claus,[68] J. P. Coleman,[68] M. R. Convery,[68] J. C. Dingfelder,[68] J. Dorfan,[68] G. P. Dubois-Felsmann,[68] D. Dujmic,[68] W. Dunwoodie,[68] R. C. Field,[68] T. Glanzman,[68] S. J. Gowdy,[68] M. T. Graham,[68] P. Grenier,[68] C. Hast,[68] T. Hryn'ova,[68] W. R. Innes,[68] J. Kaminski,[68] M. H. Kelsey,[68] H. Kim,[68] P. Kim,[68] M. L. Kocian,[68] D. W. G. S. Leith,[68] S. Li,[68] S. Luitz,[68] V. Luth,[68] H. L. Lynch,[68] D. B. MacFarlane,[68] H. Marsiske,[68] R. Messner,[68] D. R. Muller,[68] C. P. O'Grady,[68] I. Ofte,[68] A. Perazzo,[68] M. Perl,[68] T. Pulliam,[68] B. N. Ratcliff,[68] A. Roodman,[68] A. A. Salnikov,[68] R. H. Schindler,[68] J. Schwiening,[68] A. Snyder,[68] J. Stelzer,[68] D. Su,[68] M. K. Sullivan,[68] K. Suzuki,[68] S. K. Swain,[68] J. M. Thompson,[68] J. Va'vra,[68] N. van Bakel,[68] A. P. Wagner,[68] M. Weaver,[68] W. J. Wisniewski,[68] M. Wittgen,[68] D. H. Wright,[68] A. K. Yarritu,[68] K. Yi,[68] C. C. Young,[68] P. R. Burchat,[69] A. J. Edwards,[69] S. A. Majewski,[69] B. A. Petersen,[69] L. Wilden,[69] S. Ahmed,[70] M. S. Alam,[70] R. Bula,[70] J. A. Ernst,[70] V. Jain,[70] B. Pan,[70] M. A. Saeed,[70] F. R. Wappler,[70] S. B. Zain,[70] W. Bugg,[71] M. Krishnamurthy,[71] S. M. Spanier,[71] R. Eckmann,[72] J. L. Ritchie,[72] A. M. Ruland,[72] C. J. Schilling,[72] R. F. Schwitters,[72] J. M. Izen,[73] X. C. Lou,[73] S. Ye,[73] F. Bianchi,[74] F. Gallo,[74] D. Gamba,[74] M. Pelliccioni,[74] M. Bomben,[75] L. Bosisio,[75] C. Cartaro,[75] F. Cossutti,[75] G. Della Ricca,[75] L. Lanceri,[75] L. Vitale,[75] V. Azzolini,[76] N. Lopez-March,[76] F. Martinez-Vidal,[76] D. A. Milanes,[76] A. Oyanguren,[76] J. Albert,[77] Sw. Banerjee,[77] B. Bhuyan,[77] K. Hamano,[77] R. Kowalewski,[77] I. M. Nugent,[77] J. M. Roney,[77] R. J. Sobie,[77] J. J. Back,[78] P. F. Harrison,[78] T. E. Latham,[78] G. B. Mohanty,[78] M. Pappagallo,[78,§] H. R. Band,[79] X. Chen,[79] S. Dasu,[79] K. T. Flood,[79] J. J. Hollar,[79] P. E. Kutter,[79] Y. Pan,[79] M. Pierini,[79] R. Prepost,[79] S. L. Wu,[79] Z. Yu,[79] and H. Neal[80]

(*BaBar* Collaboration)

[1]*Laboratoire de Physique des Particules, IN2P3/CNRS et Université de Savoie, F-74941 Annecy-Le-Vieux, France*
[2]*Universitat de Barcelona, Facultat de Fisica, Departament ECM, E-08028 Barcelona, Spain*
[3]*Università di Bari, Dipartimento di Fisica and INFN, I-70126 Bari, Italy*
[4]*University of Bergen, Institute of Physics, N-5007 Bergen, Norway*
[5]*Lawrence Berkeley National Laboratory and University of California, Berkeley, California 94720, USA*
[6]*University of Birmingham, Birmingham, B15 2TT, United Kingdom*
[7]*Ruhr Universität Bochum, Institut für Experimentalphysik 1, D-44780 Bochum, Germany*
[8]*University of Bristol, Bristol BS8 1TL, United Kingdom*
[9]*University of British Columbia, Vancouver, British Columbia, Canada V6T 1Z1*
[10]*Brunel University, Uxbridge, Middlesex UB8 3PH, United Kingdom*
[11]*Budker Institute of Nuclear Physics, Novosibirsk 630090, Russia*
[12]*University of California at Irvine, Irvine, California 92697, USA*
[13]*University of California at Los Angeles, Los Angeles, California 90024, USA*
[14]*University of California at Riverside, Riverside, California 92521, USA*
[15]*University of California at San Diego, La Jolla, California 92093, USA*
[16]*University of California at Santa Barbara, Santa Barbara, California 93106, USA*
[17]*University of California at Santa Cruz, Institute for Particle Physics, Santa Cruz, California 95064, USA*
[18]*California Institute of Technology, Pasadena, California 91125, USA*
[19]*University of Cincinnati, Cincinnati, Ohio 45221, USA*
[20]*University of Colorado, Boulder, Colorado 80309, USA*
[21]*Colorado State University, Fort Collins, Colorado 80523, USA*
[22]*Universität Dortmund, Institut für Physik, D-44221 Dortmund, Germany*
[23]*Technische Universität Dresden, Institut für Kern- und Teilchenphysik, D-01062 Dresden, Germany*
[24]*Laboratoire Leprince-Ringuet, CNRS/IN2P3, Ecole Polytechnique, F-91128 Palaiseau, France*
[25]*University of Edinburgh, Edinburgh EH9 3JZ, United Kingdom*
[26]*Università di Ferrara, Dipartimento di Fisica and INFN, I-44100 Ferrara, Italy*
[27]*Laboratori Nazionali di Frascati dell'INFN, I-00044 Frascati, Italy*
[28]*Università di Genova, Dipartimento di Fisica and INFN, I-16146 Genova, Italy*
[29]*Harvard University, Cambridge, Massachusetts 02138, USA*
[30]*Universität Heidelberg, Physikalisches Institut, Philosophenweg 12, D-69120 Heidelberg, Germany*

[31]*Imperial College London, London, SW7 2AZ, United Kingdom*
[32]*University of Iowa, Iowa City, Iowa 52242, USA*
[33]*Iowa State University, Ames, Iowa 50011-3160, USA*
[34]*Johns Hopkins University, Baltimore, Maryland 21218, USA*
[35]*Universität Karlsruhe, Institut für Experimentelle Kernphysik, D-76021 Karlsruhe, Germany*
[36]*Laboratoire de l'Accélérateur Linéaire, IN2P3/CNRS et Université Paris-Sud 11,*
Centre Scientifique d'Orsay, B. P. 34, F-91898 ORSAY Cedex, France
[37]*Lawrence Livermore National Laboratory, Livermore, California 94550, USA*
[38]*University of Liverpool, Liverpool L69 7ZE, United Kingdom*
[39]*Queen Mary, University of London, E1 4NS, United Kingdom*
[40]*University of London, Royal Holloway and Bedford New College, Egham, Surrey TW20 0EX, United Kingdom*
[41]*University of Louisville, Louisville, Kentucky 40292, USA*
[42]*University of Manchester, Manchester M13 9PL, United Kingdom*
[43]*University of Maryland, College Park, Maryland 20742, USA*
[44]*University of Massachusetts, Amherst, Massachusetts 01003, USA*
[45]*Massachusetts Institute of Technology, Laboratory for Nuclear Science, Cambridge, Massachusetts 02139, USA*
[46]*McGill University, Montréal, Québec, Canada H3A 2T8*
[47]*Università di Milano, Dipartimento di Fisica and INFN, I-20133 Milano, Italy*
[48]*University of Mississippi, University, Mississippi 38677, USA*
[49]*Université de Montréal, Physique des Particules, Montréal, Québec, Canada H3C 3J7*
[50]*Mount Holyoke College, South Hadley, Massachusetts 01075, USA*
[51]*Università di Napoli Federico II, Dipartimento di Scienze Fisiche and INFN, I-80126, Napoli, Italy*
[52]*NIKHEF, National Institute for Nuclear Physics and High Energy Physics, NL-1009 DB Amsterdam, The Netherlands*
[53]*University of Notre Dame, Notre Dame, Indiana 46556, USA*
[54]*Ohio State University, Columbus, Ohio 43210, USA*
[55]*University of Oregon, Eugene, Oregon 97403, USA*
[56]*Università di Padova, Dipartimento di Fisica and INFN, I-35131 Padova, Italy*
[57]*Laboratoire de Physique Nucléaire et de Hautes Energies, IN2P3/CNRS, Université Pierre et Marie Curie-Paris6,*
Université Denis Diderot-Paris7, F-75252 Paris, France
[58]*University of Pennsylvania, Philadelphia, Pennsylvania 19104, USA*
[59]*Università di Perugia, Dipartimento di Fisica and INFN, I-06100 Perugia, Italy*
[60]*Università di Pisa, Dipartimento di Fisica, Scuola Normale Superiore and INFN, I-56127 Pisa, Italy*
[61]*Prairie View A&M University, Prairie View, Texas 77446, USA*
[62]*Princeton University, Princeton, New Jersey 08544, USA*
[63]*Università di Roma La Sapienza, Dipartimento di Fisica and INFN, I-00185 Roma, Italy*
[64]*Universität Rostock, D-18051 Rostock, Germany*
[65]*Rutherford Appleton Laboratory, Chilton, Didcot, Oxon, OX11 0QX, United Kingdom*
[66]*DSM/Dapnia, CEA/Saclay, F-91191 Gif-sur-Yvette, France*
[67]*University of South Carolina, Columbia, South Carolina 29208, USA*
[68]*Stanford Linear Accelerator Center, Stanford, California 94309, USA*
[69]*Stanford University, Stanford, California 94305-4060, USA*
[70]*State University of New York, Albany, New York 12222, USA*
[71]*University of Tennessee, Knoxville, Tennessee 37996, USA*
[72]*University of Texas at Austin, Austin, Texas 78712, USA*
[73]*University of Texas at Dallas, Richardson, Texas 75083, USA*
[74]*Università di Torino, Dipartimento di Fisica Sperimentale and INFN, I-10125 Torino, Italy*
[75]*Università di Trieste, Dipartimento di Fisica and INFN, I-34127 Trieste, Italy*
[76]*IFIC, Universitat de Valencia-CSIC, E-46071 Valencia, Spain*
[77]*University of Victoria, Victoria, British Columbia, Canada V8W 3P6*
[78]*Department of Physics, University of Warwick, Coventry CV4 7AL, United Kingdom*
[79]*University of Wisconsin, Madison, Wisconsin 53706, USA*
[80]*Yale University, New Haven, Connecticut 06511, USA*

(Received 31 March 2007; published 24 September 2007)

The shape of the hadronic form factor $f_+(q^2)$ in the decay $D^0 \to K^- e^+ \nu_e$ has been measured in a model independent analysis and compared with theoretical calculations. We use 75 fb^{-1} of data recorded

---

[*] Deceased.

[†] Also with Università di Perugia, Dipartimento di Fisica, Perugia, Italy.

[‡] Also with Università della Basilicata, Potenza, Italy.

[§] Also with IPPP, Physics Department, Durham University, Durham DH1 3LE, United Kingdom.

by the *BABAR* detector at the PEP-II electron-positron collider. The corresponding decay branching fraction, relative to the decay $D^0 \to K^- \pi^+$, has also been measured to be $R_D = \mathcal{B}(D^0 \to K^- e^+ \nu_e(\gamma))/\mathcal{B}(D^0 \to K^- \pi^+(\gamma)) = 0.927 \pm 0.007 \pm 0.012$. From these results, and using the present world average value for $\mathcal{B}(D^0 \to K^- \pi^+)$, the normalization of the form factor at $q^2 = 0$ is determined to be $f_+(0) = 0.727 \pm 0.007 \pm 0.005 \pm 0.007$ where the uncertainties are statistical, systematic, and from external inputs, respectively.

DOI: 10.1103/PhysRevD.76.052005 PACS numbers: 13.25.Hw, 11.30.Er, 12.15.Hh

I. INTRODUCTION

Measurements of exclusive semileptonic D decays provide an accurate determination of the hadronic form factors entering in these decays. Assuming that the CKM matrix is unitary, the elements $|V_{cs}|$ and $|V_{cd}|$ can be determined:

$$|V_{cs}| = |V_{ud}| - \frac{|V_{cb}|^2}{2} + \mathcal{O}(\lambda^6) = 0.9729 \pm 0.0003, \quad (1)$$

using the measured values [1] of $|V_{ud}|$ and $|V_{cb}|$, and the sine of the Cabibbo angle $\lambda = \sin(\theta_c) \simeq 0.227$. Theoretical predictions give estimates of the form factors in exclusive semileptonic B and D meson decays. Precise measurements of the hadronic form factors in D decays can help to validate predictions from QCD calculations in both D and B decays. Better understanding of the form factors in B decays is necessary to improve the precision on the determination of $|V_{cb}|$ and $|V_{ub}|$.

In $D^0 \to K^- e^+ \nu_e$ decays [2], with a pseudoscalar hadron emitted in the final state, and neglecting the electron mass, the differential decay rate depends only on one form factor $f_+(q^2)$,

$$\frac{d\Gamma}{dq^2} = \frac{G_F^2}{24\pi^3} |V_{cs}|^2 |\vec{p}_K(q^2)|^3 |f_+(q^2)|^2, \quad (2)$$

where G_F is the Fermi constant, q^2 is the invariant mass squared of the two leptons, e^+ and ν_e, and $\vec{p}_K(q^2)$ is the kaon three-momentum in the D^0 rest frame [3]. In this paper we present measurements of the q^2 variation and absolute value of the hadronic form factor at $q^2 = 0$ for the decay $D^0 \to K^- e^+ \nu_e(\gamma)$. The data consist of D mesons produced in $e^+e^- \to c\bar{c}$ continuum events at a center of mass energy near the $\Upsilon(4S)$ mass, and were recorded by the *BABAR* detector at the Stanford Linear Accelerator Center's PEP-II collider. A semi-inclusive reconstruction technique is used to select charm semileptonic decays with high efficiency. As a result of this approach, events with a photon radiated during the D^0 decay are included in the signal. The systematic uncertainties are kept as low as possible by using control samples extracted from data where possible.

Measurements of $D \to K \bar{\ell} \nu_\ell$, based on smaller signal events samples, have been published by the CLEO [4], FOCUS [5], and Belle [6] Collaborations. FOCUS (E831) is a Fermilab heavy flavour photoproduction experiment whereas CLEO and Belle have analyzed events from e^+e^- annihilation at an energy close to the $\Upsilon(4S)$ mass. This paper is organized as follows. A general description of the hadronic form factor, $f_+(q^2)$, is given in Sec. II, where the different parameterizations considered in this analysis are explained. In Section III a short description of the detector components that are important to this measurement is given. The selection of signal events and the rejection of background are considered in Section IV. In Section V, the measured q^2 variation of the hadronic form factor is discussed and compared with previous measurements. In Sec. VI the measured decay rate is given and in Sec. VII these measurements are combined to obtain the value of $f_+(0)$.

II. THE $F_+(Q^2)$ HADRONIC FORM FACTOR

The amplitude for the decay $D^0 \to K^- \ell^+ \nu_\ell$ depends on two hadronic form factors:

$$\langle K(p')|V_\mu|D(p)\rangle = \left(p_\mu + p'_\mu - q_\mu \frac{m_D^2 - m_K^2}{q^2}\right) f_+(q^2) + \frac{m_D^2 - m_K^2}{q^2} q_\mu f_0(q^2), \quad (3)$$

where $V_\mu = \bar{s}\gamma_\mu c$. The constraint $f_+(0) = f_0(0)$ ensures that there is no singularity at $q^2 = 0$. When the charged lepton is an electron, the contribution from f_0 is proportional to m_e^2 and can be neglected in decay rate measurements.

The parameterizations of $f_+(q^2)$ which have been compared with present measurements and a few examples of theoretical approaches, proposed to determine the values of corresponding parameters, are considered in the following.

A. Form-factor parameterizations

The most general expressions of the form factor $f_+(q^2)$ are analytic functions satisfying the dispersion relation:

$$f_+(q^2) = \frac{\mathrm{Res}(f_+)_{q^2 = m_{D_s^*}^2}}{m_{D_s^*}^2 - q^2} + \frac{1}{\pi} \int_{t_+}^{\infty} dt \frac{\mathrm{Im}(f_+(t))}{t - q^2 - i\epsilon}. \quad (4)$$

The only singularities in the complex $t \equiv q^2$ plane originate from the interaction of the charm and the strange quarks in vector states. They are a pole, situated at the D_s^* mass squared and a cut, along the positive real axis, starting at threshold ($t_+ = (m_D + m_K)^2$) for D^0K^- production.

1. Taylor expansion

This cut t-plane can be mapped onto the open unit disk with center at $t = t_0$ using the variable:

$$z(t, t_0) = \frac{\sqrt{t_+ - t} - \sqrt{t_+ - t_0}}{\sqrt{t_+ - t} + \sqrt{t_+ - t_0}}. \tag{5}$$

In this variable, the physical region for the semileptonic decay ($0 < t < t_- = q^2_{\max} = (m_D - m_K)^2$) corresponds to a real segment extending between $\pm z_{\max} = \pm 0.051$. This value of $z_{\max}$ is obtained for $t_0 = t_+(1 - \sqrt{1 - t_-/t_+})$. The z expansion of f_+ is thus expected to converge quickly. The most general parameterization [7], consistent with constraints from QCD, is

$$f_+(t) = \frac{1}{P(t)\Phi(t, t_0)} a_0(t_0)\left(1 + \sum_{k=1}^{\infty} r_k(t_0) z^k(t, t_0)\right), \tag{6}$$

which is based on earlier considerations [8]. The function $P(t) = z(t, m^2_{D_s^*})$ has a zero at the D_s^* pole mass and $|P| = 1$ along the unit circle; Φ is given by

$$\begin{aligned}\Phi(t, t_0) = &\sqrt{\frac{1}{24\pi\chi_V}}\left(\frac{t_+ - t}{t_+ - t_0}\right)^{1/4}(\sqrt{t_+ - t} + \sqrt{t_+})^{-5} \\ &\times (\sqrt{t_+ - t} + \sqrt{t_+ - t_0})(\sqrt{t_+ - t} + \sqrt{t_+ - t_-})^{3/2} \\ &\times (t_+ - t)^{3/4},\end{aligned} \tag{7}$$

where χ_V can be obtained from dispersion relations using perturbative QCD and depends on $u = m_s/m_c$ [9]. At leading order, with $u = 0$ [10],

$$\chi_V = \frac{3}{32\pi^2 m_c^2}. \tag{8}$$

The choice of P and Φ is such that

$$a_0^2(t_0)\left(1 + \sum_{k=1}^{\infty} r_k^2(t_0)\right) \leq 1. \tag{9}$$

Having measured the first coefficients of this expansion, Eq. (9) can constrain the others. This constraint, which depends on χ_V, may have to be abandoned in the case of charm decays as the charm-quark mass may not be large enough to prevent the previous evaluation of χ_V from receiving large $1/m_c$ and QCD corrections. However the parameterization given in Eq. (6) remains valid and it has been compared [7] with available measurements. The first two terms in the expansion were sufficient to describe the data.

2. Model-dependent parameterizations

A less general approach assumes that the q^2 variation of $f_+(q^2)$ is governed mainly by the D_s^* pole and that the other contributions can be accounted for by adding another effective pole at a higher mass [11]:

$$\begin{aligned}f_+(q^2) &= \frac{f_+(0)}{1 - \alpha_{\text{pole}}}\left(\frac{1}{1 - \frac{q^2}{m^2_{D_s^*}}} - \frac{\alpha_{\text{pole}}}{1 - \frac{q^2}{\gamma_{\text{pole}} m^2_{D_s^*}}}\right) \\ &= f_+(0)\frac{1 - \delta_{\text{pole}}\frac{q^2}{m^2_{D_s^*}}}{(1 - \frac{q^2}{m^2_{D_s^*}})(1 - \beta_{\text{pole}}\frac{q^2}{m^2_{D_s^*}})}\end{aligned} \tag{10}$$

with $\delta_{\text{pole}} = (1/\gamma_{\text{pole}} - \alpha_{\text{pole}})/(1 - \alpha_{\text{pole}})$ and $\beta_{\text{pole}} = 1/\gamma_{\text{pole}}$.

If in addition, the form factors f_+ and f_0 must obey a relation, valid at large recoil and in the heavy quark limit, then $\alpha_{\text{pole}} = 1/\gamma_{\text{pole}}$ [11] ($\beta_{\text{pole}} = \alpha_{\text{pole}}$ and $\delta_{\text{pole}} = 0$ in this case). Equation (10) becomes:

$$f_+(q^2) = \frac{f_+(0)}{(1 - \frac{q^2}{m^2_{D_s^*}})(1 - \alpha_{\text{pole}}\frac{q^2}{m^2_{D_s^*}})}, \tag{11}$$

known as the modified pole ansatz. Initially an even simpler expression, the simple pole ansatz, was proposed which considered only the contribution from the D_s^* pole. In the following, the pole mass entering in

$$f_+(q^2) = \frac{f_+(0)}{1 - \frac{q^2}{m^2_{\text{pole}}}} \tag{12}$$

is fitted. Note that such an effective pole mass value has no clear physical interpretation and that the proposed q^2 variation does not comply with constraints from QCD. The obtained value may nonetheless be useful for comparison with results from different experiments.

B. Quantitative expectations

Values of the parameters that determine $f_+(q^2)$ were obtained initially from constituent quark models and from QCD sum rules. These two approaches have an intrinsically limited accuracy. In this respect, results from lattice QCD computations are more promising because their accuracy is mainly limited by available computing resources.

1. Quark models

Quark model calculations estimate meson wave functions and use them to compute the matrix elements that appear in the hadronic current. There are a large variety of theoretical calculations [12]. Among these models we have selected the ISGW model [13], simply because it is widely used to simulate heavy hadron semileptonic decays. This model was expected to be valid in the vicinity of $q^2_{\max}$, a region of maximum overlap between the initial and final meson wave functions. In ISGW2 [14] the exponential q^2 dependence of the form factor has been replaced by another parameterization, with a dipole behavior, expected to be valid over a larger q^2 range:

$$f_+^{\mathrm{ISGW2}}(q^2) = \frac{f_+(q^2_{\mathrm{max}})}{(1+\alpha_I(q^2_{\mathrm{max}}-q^2))^2}, \qquad \alpha_I = \frac{1}{12}r^2. \quad (13)$$

The predicted values of the parameters are $f_+(q^2_{\mathrm{max}}) = 1.23$ and $r = 1.12\ \mathrm{GeV}^{-1}$ for the charge radius [14].

2. *QCD sum rules*

QCD sum rules [15] and their extension on the light cone [16], are expected to be valid at low q^2. Using a value of 150 MeV for the strange quark mass, one obtains [16]:

$$f_+(0) = 0.78 \pm 0.11 \quad \text{and} \quad \alpha_{\mathrm{pole}} = -0.07^{+0.15}_{-0.07}, \quad (14)$$

using the modified pole ansatz. The uncertainty of $f_+(0)$ is estimated to be of order 15%, and the q^2 dependence is expected to be dominated by a single pole at the D_s^* mass because the value of α_{pole} is compatible with zero.

3. *Lattice QCD*

Lattice QCD computation is the only approach able to compute $f_+(q^2)$ from first principles. Current results must be extrapolated to physical values of light-quark masses and corrected for finite lattice size and discritization effects. There have been several evaluations of $f_+(q^2)$ for different values of the momentum transfer in the quenched approximation [17,18]. These results have been combined [17], giving $f_+(0) = 0.73 \pm 0.07$. The first unquenched calculation has been published recently [19]: $f_+(0) = 0.73 \pm 0.03 \pm 0.07$ and $\alpha_{\mathrm{pole}} = 0.50 \pm 0.04$, using the modified pole ansatz to parameterized the q^2 dependence of the form factor.

C. Analyzed parameterizations

The different parameterizations of $f_+(q^2)$ considered in this analysis are summarized in Table I, along with their corresponding parameters and expected values, where available.

III. THE *BABAR* DETECTOR AND DATASET

A detailed description of the *BABAR* detector [20] and of the algorithms used for charged and neutral particle reconstruction and identification [21] is provided elsewhere. Charged particles are reconstructed by matching hits in the 5-layer double-sided silicon vertex tracker (SVT) with track elements in the 40-layer drift chamber (DCH), which is filled with a gas mixture of helium and isobutane. Low momentum particles which do not leave enough hits in the DCH due to the bending in the 1.5 T magnetic field, are reconstructed in the SVT. Charged hadron identification is performed combining the measurements of the energy deposition in the SVT and in the DCH with the information from the Cherenkov detector (DIRC). Photons are detected and measured in the CsI(Tl) electro-magnetic calorimeter (EMC). Electrons are identified by the ratio of the track momentum to the associated energy deposited in the EMC, the transverse profile of the shower, the energy loss in the DCH, and the Cherenkov angle in the DIRC. Muons are identified in the instrumented flux return, composed of resistive plate chambers interleaved with layers of steel and brass.

TABLE I. Parameterizations of $f_+(q^2)$.

Modeling	Parameters	Expected values
z expansion [8]	a_0, r_k, $k \geq 1$	No prediction
General two poles [11]	$f_+(0)$, β_{pole}, δ_{pole}	No prediction
Modified pole [11]	$f_+(0)$, α_{pole}	$\delta_{\mathrm{pole}} = 0$
Simple pole	$f_+(0)$, m_{pole}	$m_{\mathrm{pole}} = m_{D_s^*}$
ISGW2 [14]	$f_+(t_-)$, α_I	$f_+(t_-) = 1.23$ $\alpha_I = 0.104\ \mathrm{GeV}^{-2}$

The results presented here are obtained using a total integrated luminosity of $75\ \mathrm{fb}^{-1}$ registered by the *BABAR* detector during the years 2000–2002. Monte Carlo (MC) simulation samples of $\Upsilon(4S)$ decays, charm and other light-quark pairs from continuum equivalent, respectively, to 2.8, 1.2 and 0.7 times the data statistics, respectively, have been generated using GEANT4 [22]. These are used mainly to evaluate background components. Quark fragmentation, in continuum events, is described using the JETSET package [23]. The MC distributions have been rescaled to the data sample luminosity, using the expected cross sections of the different components (1.3 nb for $c\bar{c}$, 0.525 nb for B^+B^- and $B^0\bar{B}^0$, 2.09 nb for light $u\bar{u}$, $d\bar{d}$ and $s\bar{s}$ quark events). Dedicated MC samples of pure signal events, equivalent to 7 times the data statistics, are used to correct measurements for efficiency and finite resolution effects. They have been generated using the modified pole parameterization ansatz for $f_+(q^2)$ with $\alpha_{\mathrm{pole}} = 0.50$. Radiative decays ($D^0 \to K^- e^+ \nu_e \gamma$) are modeled by PHOTOS [24]. To account for one of the most important sources of background, a special event sample with, in each event, at least one cascade decay $D^{*+} \to D^0 \pi^+$, $D^0 \to K^- \pi^0 e^+ \nu_e$ (or its charge conjugate) has been generated with a parameterization of the form factors in agreement with measurements from the FOCUS Collaboration [25]. Events with a D^{*+} and a D^0 decaying into $K^-\pi^+$ or $K^-\pi^+\pi^0$ have been reconstructed in data and simulation. These control samples have been used to adjust the c-quark fragmentation distribution and the kinematic characteristics of particles accompanying the D meson in order to better match the data. They have been used also to measure the reconstruction accuracy on the missing neutrino momentum. In addition, $K^-\pi^+$ events are used as a reference channel in the $D^0 \to K^- e^+ \nu_e(\gamma)$ branching fraction measurement.

IV. SIGNAL RECONSTRUCTION

We reconstruct $D^0 \to K^- e^+ \nu_e(\gamma)$ decays in $e^+e^- \to c\bar{c}$ events where D^0 originates from the $D^{*+} \to D^0 \pi^+$. The main sources of background arise from events with a kaon and electron candidate. Such events come from $\Upsilon(4S)$ decays and the continuum production of charmed hadrons. Their contribution is reduced using variables sensitive to the particle production characteristics that are different for signal and background events.

A. Signal selection

Charged and neutral particles are boosted to the center of mass system (c.m.) and the event thrust axis is determined. The direction of this axis is required to be in the interval $|\cos(\theta_{\mathrm{thrust}})| < 0.6$ to minimize the loss of particles in regions close to the beam axis. A plane perpendicular to the thrust axis is used to define two hemispheres, equivalent to the two jets produced by quark fragmentation. In each hemisphere, we search for pairs of oppositely charged leptons and kaons. For the charged lepton candidates we consider only electrons or positrons with c.m. momentum greater than 0.5 GeV/c.

Since the ν_e momentum is unmeasured, a kinematic fit is performed, constraining the invariant mass of the candidate $K^- e^+ \nu_e$ system to the D^0 mass. In this fit, the D^0 momentum and the neutrino energy are estimated from the other, charged and neutral, particles measured in the event. Masses of charged particles are assigned according to the information provided by particle identification algorithms. The D^0 direction is taken as the direction opposite to the sum of the momenta of all reconstructed particles in the event, except for the kaon and the positron associated with the signal candidate. The energy of the jet is determined from the total c.m. energy and from the measured masses of the two jets. The neutrino energy is estimated as the difference between the total energy of the jet containing the kaon and the electron and the sum of the particle energies in that hemisphere. A correction, which depends on the value of the missing energy measured in the opposite jet, is applied to account for the presence of missing energy due to particles escaping detection, even in the absence of a neutrino from the D^0 decay.

The D^0 candidate is retained if the χ^2 probability of the kinematic fit exceeds 10^{-3}. Detector performance for the reconstruction of the D^0 direction and for the missing energy are measured using events in which the D^0 decays into $K^-\pi^+$. Corrections are applied to account for observed differences between data and simulation. Each D^0 candidate is combined with a charged pion, with the same charge as the lepton, and situated in the same hemisphere. The mass difference $\delta(m) = m(D^0\pi^+) - m(D^0)$ is evaluated and is shown in Fig. 1. This distribution contains events which in addition pass the requirements on the Fisher discriminant $F_{B\bar{B}}$ suppressing $B\bar{B}$ background and also give a satisfactory kinematic fit constraining the invariant D^* mass which is described in Section IV C. This last requirement is the reason of the slow decrease of the $\delta(m)$ distribution. At large $\delta(m)$ values, there is a small excess of background in data and the simulation is rescaled accordingly, in Sec. VA 5, to determine the signal component. Only events with $\delta(m) < 0.16$ GeV/c^2 are used in the analysis.

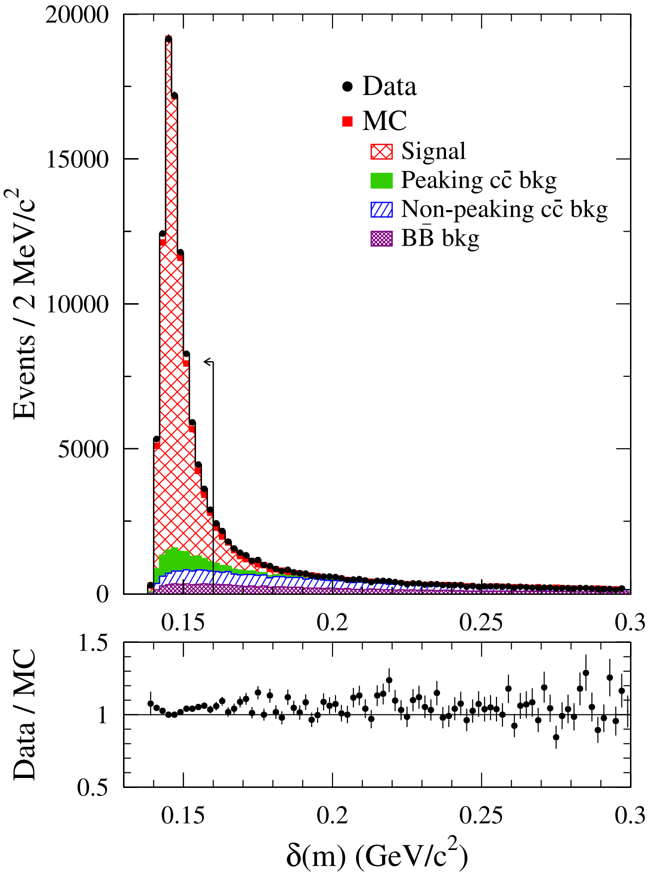

FIG. 1 (color online). Comparison of the $\delta(m)$ distributions from data and simulated events. MC events have been normalized to the sample luminosity according to the different cross sections. An excess of background events of the order of 5% is observed for large values of $\delta(m)$. The background component expected from light quarks is not visible with this scale. The arrow indicates the additional selection applied for the q^2 distribution measurement.

B. Background rejection

Background events arise from $\Upsilon(4S)$ decays and hadronic events from the continuum. Three variables are used to reduce the contribution from $B\bar{B}$ events: R_2 (the ratio between the second and zeroth order Fox-Wolfram moments [26]), the total charged and neutral multiplicity and the momentum of the soft pion (π_s) from the D^{*+}.

These variables exploit the topological differences between events with B decays and events with $c\bar{c}$ fragmentation. The particle distribution in $\Upsilon(4S)$ decay events tends to be isotropic as the B mesons are produced near threshold, while the distribution in $c\bar{c}$ events is jetlike as the c.m. energy is well above the charm threshold. This also results in a softer D^{*+} momentum spectrum in $\Upsilon(4S)$ decays compared to $c\bar{c}$ events.

Corresponding distributions of these variables for signal and background events are given in Fig. 2. These variables have been combined linearly in a Fisher discriminant. The requirement $F_{B\bar{B}} > 0.5$ retains 65% of signal and 6% of $B\bar{B}$-background events.

Background events from the continuum arise mainly from charm particles as requiring an electron and a kaon reduces the contribution from light-quark flavors to a low level. Because charm hadrons take a large fraction of the charm-quark energy charm decay products have higher average energies and different angular distributions (relative to the thrust axis or to the D direction) compared with other particles in the hemisphere emitted from the hadronization of the c and $\bar{c}$ quarks. These other particles are referred to as "spectator" in the following; the "leading" particle is the one with the largest momentum. To reduce background from $c\bar{c}$ events, the following variables are used:

(i) the D^0 momentum;
(ii) the spectator system mass, m_{sp}, which has lower values for signal events;
(iii) the direction of the spectator system momentum relative to the thrust axis $\cos\theta_{\mathrm{sp\text{-}thrust}}$;
(iv) the momentum of the leading spectator track;
(v) the direction of the leading spectator track relative to the D^0 direction;
(vi) the direction of the leading spectator track relative to the thrust axis;
(vii) the direction of the lepton relative to the kaon direction, in the $e^+\nu_e$ rest frame, $\cos\theta_e$;
(viii) the charged lepton momentum, $|\vec{p}_e|$, in the c.m. frame.

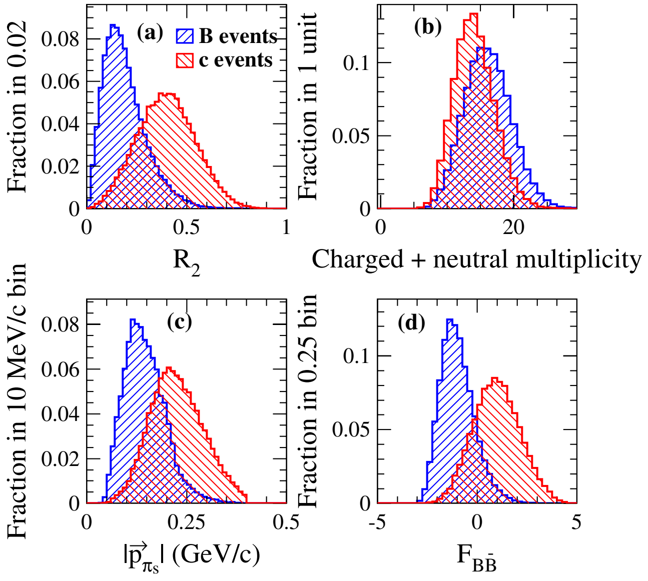

FIG. 2 (color online). MC simulations of distributions of the variables used in the Fisher discriminant analysis to reduce the $B\bar{B}$ event background: (a) the normalized second Fox-Wolfram moment (R_2), (b) the event particle multiplicity, (c) the slow-pion momentum distribution, in the c.m. frame, (d) the Fisher variable for $B\bar{B}$ and for charm signal events.

The first six variables depend on the properties of c-quark hadronization whereas the last two are related to decay characteristics of the signal. Distributions for four of the most discriminating variables are given in Fig. 3. $D^0 \to K^-\pi^+$ events have been used to tune the simulation parameters so that distributions of the variables used to reject background agree with those measured with data events. These eight variables have been combined linearly into a Fisher discriminant variable (F_{cc}) and events have been kept for values above 0. This selection retains 77% of signal events that were kept by the previous selection requirement and rejecting 66% of the background (Fig. 4).

The remaining background from $c\bar{c}$-events can be divided into peaking (60%) and nonpeaking (40%) candidates. Peaking events are those background events whose distribution is peaked around the signal region. These are mainly events with a real D^{*+} in which the slow π^+ is included in the candidate track combination. Backgrounds from e^+e^- annihilations into light $u\bar{u}$, $d\bar{d}$, $s\bar{s}$ quarks and $B\bar{B}$ events are nonpeaking. These components, from simulation, are displayed in Fig. 1.

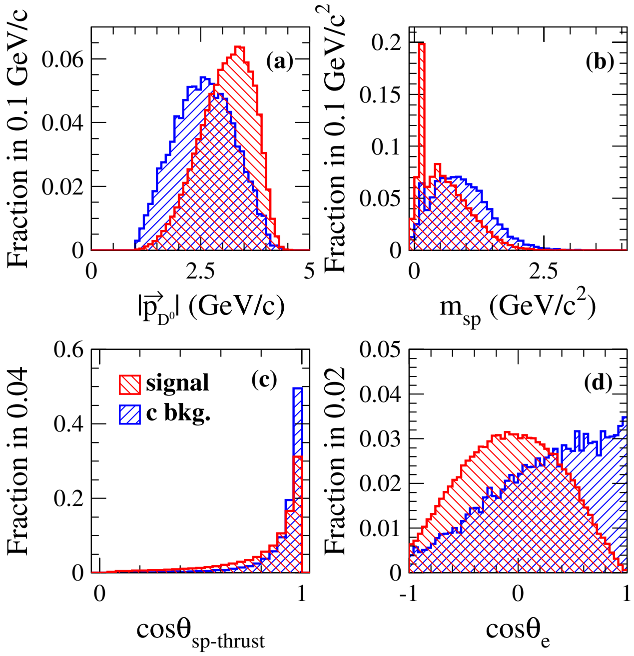

FIG. 3 (color online). MC simulations of some of the variables used in the Fisher discriminant analysis to reduce the $c\bar{c}$-event background: (a) the D^0 momentum after the kinematic fit, (b) the mass of the spectator system (peaks, at low mass values correspond to events with a single charged pion or photon reconstructed in the spectator system), (c) the cosine of the angle between the spectator system momentum and the thrust direction, (d) the cosine of the angle of the positron direction, relative to the kaon direction, in the $e\nu_e$ c.m. frame.

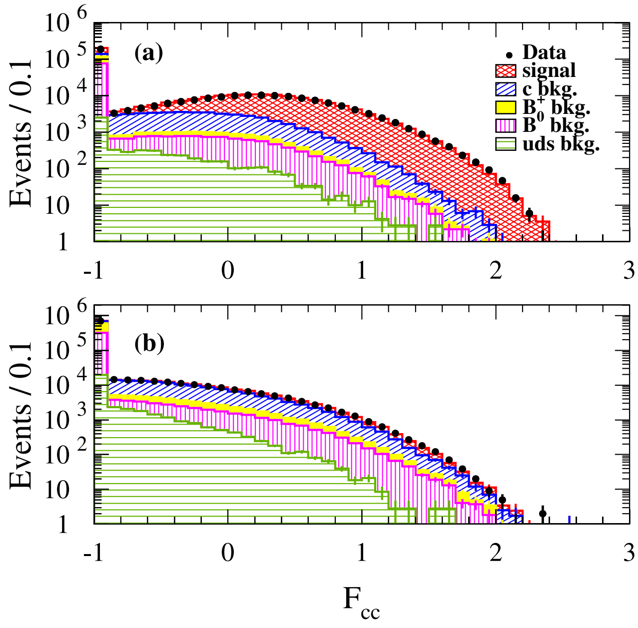

FIG. 4 (color online). Distribution of the values of the Fisher variable in the signal region ($\delta(m) < 0.16$ GeV$/c^2$ in (a), and for masses above the signal region ($\delta(m) > 0.16$ GeV$/c^2$ in (b).

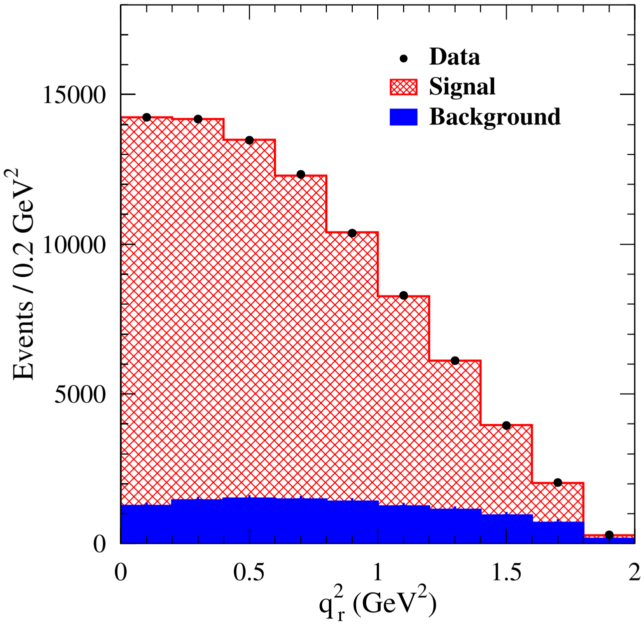

FIG. 5 (color online). The measured q_r^2 distribution (data points) compared to the sum of the estimated background and of the fitted signal components.

C. q^2 measurement

To improve the accuracy of the reconstructed D^0 momentum, the nominal D^{*+} mass is added as a constraint in the previous fit and only events with a χ^2 probability higher than 1% are kept (Fig. 1 is obtained requiring only that the fit has converged). It is verified that the sample composition of the nonpeaking background does not depend on this last condition. The measured q_r^2 distribution, where $q_r^2 = (p_D - p_K)^2$, is given in Fig. 5. There are 85 260 selected D^0 candidates containing an estimated number of 11280 background events. The nonpeaking component comprises 54% of the background.

To obtain the true q^2 distribution, the measured one has to be corrected for selection efficiency and detector resolution effects. This is done using an unfolding algorithm based on MC simulation of these effects.

The variation of the selection efficiency as a function of q^2 is given in Fig. 6. The resolution of the q^2 measurement for signal events is obtained from MC simulation. The resolution function can be fitted by the sum of two Gaussian functions, with standard deviations $\sigma_1 = 0.066$ GeV^2 and $\sigma_2 = 0.219$ GeV^2, respectively. The narrow component corresponds to 40% of the events.

To obtain the unfolded q^2 distribution for signal events, corrected for resolution and acceptance effects, the Singular Value Decomposition (SVD) [27] of the resolution matrix has been used. This method uses a two-dimensional matrix which relates the generated q^2 distribution to the detected distribution, q_r^2, as input. After subtracting the estimated background contribution, the measured binned q_r^2 distribution is linearly transformed into the unfolded q^2 distribution. This approach provides the full covariance matrix for the bin contents of the unfolded distribution. Singular values (SV) are ordered by decreasing values. These values contain the information needed to transform the measured distribution into the unfolded spectrum, along with statistical uncertainties from fluctuations. Not all SV are relevant; nonsignificant

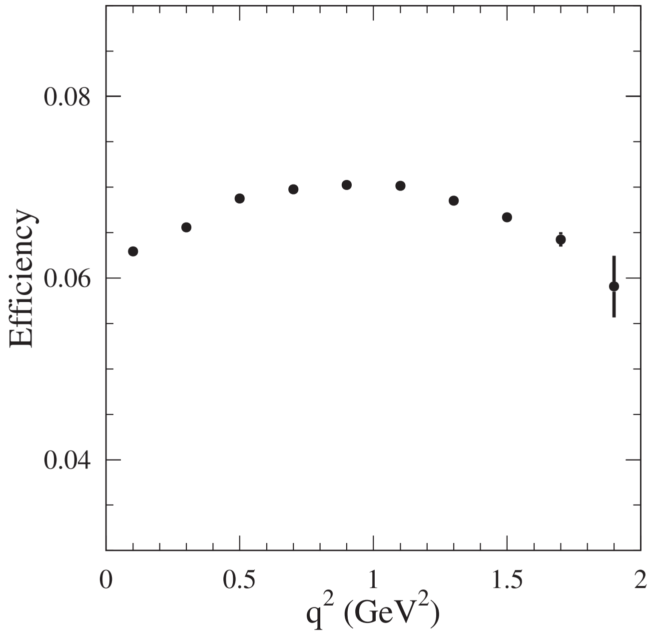

FIG. 6. The efficiency as a function of q^2, measured with simulated signal events, after all selection criteria applied.

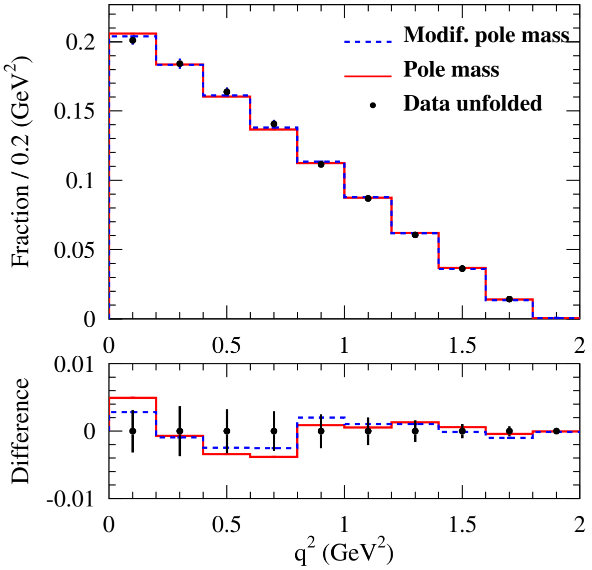

FIG. 7 (color online). Comparison between the normalized unfolded q^2 distribution obtained from this analysis, and those corresponding to two fitted models. Lower plot gives the difference between measured and fitted distributions. The error bars represent statistical errors only.

values have zero mean and standard deviation equal to unity [27]. Using toy simulations, we find that seven SV have to be kept with events distributed over ten bins in q^2. Because the measurement of the form-factor parameters relies on the measured q_r^2 distribution, it does not require unfolding, and is independent of this particular choice.

V. RESULTS ON THE q^2 DEPENDENCE OF THE HADRONIC FORM FACTOR

The unfolded q^2 distribution, normalized to unity, is presented in Fig. 7 and in Table II. Also given in this table are the statistical and total uncertainties and the correlations of the data in the ten bins. Figure 7 shows the result of fits to the data for two parameterizations of the form factor with a single free parameter, the simple pole and the modified pole ansatz. Both fitted distributions agree well with the data.

A summary of these and other form-factor parameterizations is given in Table III. These results will be discussed in detail in Sec. V B.

The fit to a model is done by comparing the number of events measured in a given bin of q^2 with the expectation from the exact analytic integration of the expression

TABLE II. Statistical and total uncertainty matrices for the normalized decay distribution (corrected for acceptance and finite resolution effects) in ten bins of q^2 from 0 to 2 GeV^2, and for the ratio R_D (see Section VI). The total decay distribution has been normalized to unity for q^2 varying over ten 0.2 GeV^2 intervals. The uncertainty matrices are provided for both the statistical (upper half) and total (lower half) uncertainties. The uncertainty on each measured value (σ_i) is given along the diagonal. Off-diagonal terms correspond to the correlation coefficients (ρ_{ij}). From this information, the error covariance matrix elements correspond to: $\sigma_{ii} = \sigma_i^2$ and $\sigma_{ij} = \rho_{ij}\sigma_i\sigma_j$ and the matrix is symmetric relative to the diagonal.

q^2 bin (GeV^2)		[0, 0.2]	[0.2, 0.4]	[0.4, 0.6]	[0.6, 0.8]	[0.8, 1.0]	[1.0, 1.2]	[1.2, 1.4]	[1.4, 1.6]	[1.6, 1.8]	[1.8, 2.0]
R_D and fractions	0.9269	0.2008	0.1840	0.1632	0.1402	0.1122	0.0874	0.0602	0.0367	0.0146	0.0007
statistical uncertainties and correlations	0.0072	0.166	0.122	0.111	0.107	0.107	0.102	0.101	0.116	0.081	0.060
		0.0031	−0.451	−0.155	0.117	0.005	0.023	0.002	0.002	−0.002	−0.002
			0.0037	−0.225	−0.304	0.095	0.041	−0.025	−0.005	0.005	−0.005
				0.0033	−0.155	−0.345	0.079	0.058	−0.018	−0.010	−0.006
					0.0029	−0.113	0.352	0.058	0.066	−0.013	−0.024
						0.0025	0.073	−0.345	0.018	0.075	0.067
							0.0020	−0.029	−0.329	−0.004	0.060
								0.0016	0.110	−0.339	−0.347
									0.0011	0.217	0.012
										0.00075	0.965
											0.000057
Total Uncertainties and Correlations	0.0139	−0.154	0.071	0.034	0.092	0.046	0.085	0.231	0.271	0.202	0.179
		0.0042	−0.449	−0.249	0.023	0.097	0.095	−0.242	−0.116	−0.085	−0.075
			0.0040	−0.094	−0.243	0.000	0.024	0.006	−0.056	−0.079	−0.071
				0.0034	−0.123	−0.374	0.046	0.067	−0.054	−0.048	−0.041
					0.0030	−0.127	0.320	0.087	0.048	−0.041	−0.050
						0.0026	0.038	−0.324	0.038	0.092	0.082
							0.0022	0.090	−0.234	0.028	0.071
								0.0018	0.179	−0.189	−0.209
									0.0012	0.416	0.252
										0.0009	0.974
											0.000069

TABLE III. Fitted parameters corresponding to different parameterizations of $f_+(q^2)$, with their statistical and systematic errors, the χ^2/NDF of the fit, compared to the predicted values and the χ^2/NDF of the fit, assuming these values.

Theoretical ansatz	Unit	Parameters	χ^2/NDF	Parameter expectation	χ^2/NDF
z expansion		$r_1 = -2.5 \pm 0.2 \pm 0.2$	5.9/7		
		$r_2 = 0.6 \pm 6. \pm 5.$			
Modified pole		$\alpha_{\mathrm{pole}} = 0.377 \pm 0.023 \pm 0.031$	6.0/8		
Simple pole	GeV/c^2	$m_{\mathrm{pole}} = 1.884 \pm 0.012 \pm 0.016$	7.4/8	2.112	243/9
ISGW2	GeV^{-2}	$\alpha_I = 0.226 \pm 0.005 \pm 0.007$	6.4/8	0.104	800/9

$|\vec{p}_K(q^2)|^3|f_+(q^2)|^2$ over the bin range, with the overall normalization left free. The result of the fit corresponding to the parameterization of the form factor using two parameters [see Eq. (10)] is given in Fig. 8.

A. Systematic uncertainties

Systematic uncertainties of the form-factor parameters are likely to originate from imperfect simulation of c-quark fragmentation and the detector response, from uncertainties in the background composition and the individual contributions for the selected signal sample, the uncertainty in the modeling of the signal decay and the measurement of the q^2 distribution. We study the origin and size of various systematic effects, correct the MC simulation, if possible, assess the impact of the uncertainty of the size of correction on the fit results, and adopt the observed change as a contribution to the systematic uncertainty on the fitted parameters for the different parameterizations under study. Some of these studies make use of standard *BABAR* evaluations of detection efficiencies, others rely on special data control samples, for instance hadronic decays $D^0 \to K^-\pi^+$ or $K^-\pi^+\pi^0$.

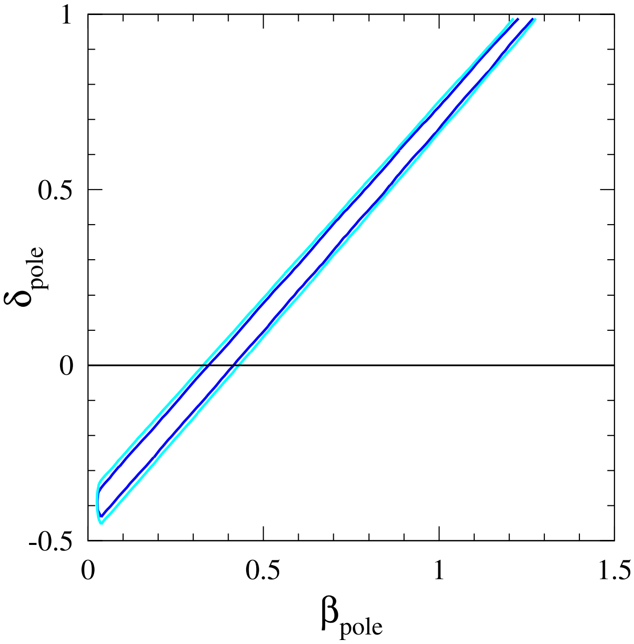

FIG. 8 (color online). Contours at 70% and 90% C.L. resulting from the fit of the parameterization of the form-factor q^2 dependence with two parameters as given in Eq. (10). The value $\delta_{\mathrm{pole}} = 0$ corresponds to the modified pole ansatz.

1. c-quark hadronization tuning

The signal selection is based on variables related to c-quark fragmentation and decay properties of signal events. Simulated events have been weighted to agree with the distributions observed in data. Weights have been obtained using events with a reconstructed D^0 decaying into $K^-\pi^+$. After applying these corrections, the distribution of the Fisher discriminant that contains these variables is compared for data and simulation. The remaining relative difference, which is below 5% over the range of this quantity, is used to evaluate the corresponding systematic uncertainty. It corresponds to the variations on fitted quantities obtained by correcting or not for this difference.

2. Reconstruction algorithm

It is important to verify that the q^2 variation of the selection efficiency is well described by the simulation. This is done by analyzing $D^0 \to K^-\pi^+\pi^0$ as if they were $K^-e^+\nu_e$ events. The two photons from the π^0 are removed and events are reconstructed using the algorithm applied to the semileptonic D^0 decay. The "missing" π^0 and the charged pion play, respectively, the roles of the neutrino and the electron. To preserve the correct kinematic limits, it is necessary to take into account that the "fake" neutrino has the π^0 mass and that the fake electron has the π^+ mass.

Data and simulated events, which satisfy the same analysis selection criteria as for $Ke\nu_e$, have been compared. For this test, the $\cos(\theta_e)$ and p_e variables are removed from the Fisher discriminant, because distributions for these two variables in $K^-\pi^+\pi^0$ events are different from the signal events.

The ratio of efficiencies measured in data and simulation is fit with a linear expression in q^2. The corresponding slope, $(0.71 \pm 0.68)\%$, indicates that there is no significant bias when the event selection criteria are applied. The measured slope is used to define a correction and to estimate the corresponding systematic uncertainty.

3. Resolution on q^2

To measure possible differences between data and simulation on the q^2 reconstruction accuracy, $D^0 \to K^- \pi^+ \pi^0$ events are used again. Distributions of the difference $q_r^2 - q^2$, obtained by selecting events in a given bin of q^2 are compared. These distributions are systematically slightly narrower for simulated events and the fraction of events in the distant tails are higher for data (see Fig. 9).

With the $D^0 \to K^- \pi^+$ sample we study, in data and simulation, the accuracy of the D^0 direction and missing energy reconstruction for the $D^0 \to K^- e^+ \nu_e$ analysis. This information is used in the mass-constrained fits and thus influences the q^2 reconstruction. Once the simulation is tuned to reproduce the results obtained on data for these parameters, the q^2 resolution distributions agree very well, as shown in Fig. 9. One half of the measured variation on the fitted parameters from these corrections has been taken as a systematic uncertainty.

4. Particle identification

Effects from a momentum-dependent difference between data and simulated events on the charged lepton and on the kaon identification have been evaluated. Such differences, which are typically below 2%, have been measured for selected, high purity samples of electrons and kaons. These corrections have been applied and the observed variation has been taken as the estimate of the systematic uncertainty.

5. Background estimate

The background under the D^{*+} signal has two components that have, respectively, nonpeaking and peaking behavior.

The nonpeaking background originates from non-$c\bar{c}$ events and from continuum charm events in which the π_s candidate does not come from a cascading D^{*+}. By comparing data and simulated event rates for $\delta(m) > 0.18\ \mathrm{GeV}/c^2$ (see Fig. 1), a correction of 1.05 is determined from simulation for the nonpeaking background. This correction is applied and an uncertainty of ±0.05 is used as the corresponding systematic uncertainty. The effect of a different variation of the nonpeaking background level with q_r^2 has been evaluated by comparing corresponding distributions in data and simulation for events selected with $\delta(m)$ between 0.18 and $0.20\ \mathrm{GeV}/c^2$. The measured difference, of ±5% over the q_r^2 range, is used to determine the corresponding systematic uncertainty.

Events which include a slow pion originating from D^{*+} decay contribute in several ways to the peaking background. The production rate of D^{*+} mesons in the simulation is in agreement with expectations based on measurements from CLEO [28]. The uncertainty of ±0.06 on this comparison is dominated by the systematic uncertainty from the CLEO result.

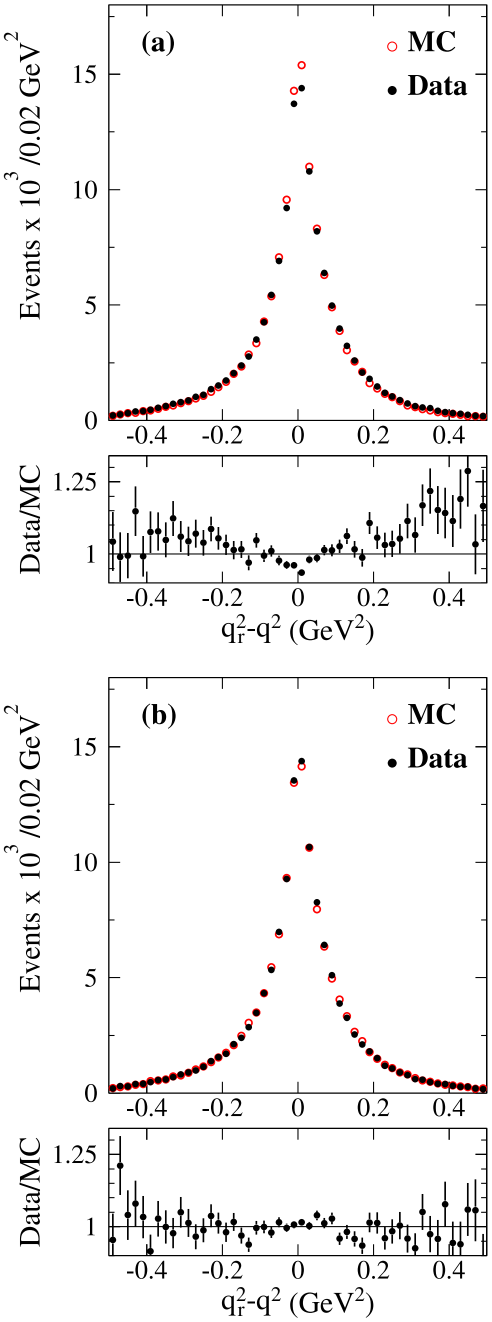

FIG. 9 (color online). Distribution of the difference between the true and the reconstructed value of q^2. $D^0 \to K^- \pi^+ \pi^0$ data events correspond to dark squares and open circles are used for simulated ones. Ratio (Data/MC) of the two distributions are displayed. The distributions in a) compare data and simulated events before applying corrections measured with $D^0 \to K^- \pi^+$ events, whereas these corrections have been applied for plots in (b).

To study the remaining effects, the peaking background components have been divided according to the process from which they originate and have been ordered by decreasing level of importance:

(i) *the K^- and the electron originate from a D^0 decay (54%)*. The main source comes from $D^0 \to K^-\pi^0 e^+ \nu_e$. We have corrected the decay branching fraction used for this channel in the MC (2.02%) using recent measurements (2.17 ± 0.16% [1]). The uncertainty on this value has been used to evaluate the corresponding systematic uncertainty.

(ii) *the electron comes from a converted photon or a Dalitz decay (24%)*. It has been assumed that the simulation correctly accounts for this component;

(iii) *the K^- does not originate from a charm hadron (14%)*. This happens usually when there is another negative charged kaon accompanying the D^{*+}. We have studied the production of charged kaon accompanying a D^{*+} using $D^0 \to K^-\pi^+$ events and measure a correction factor of 0.87 ± 0.02 and 0.53 ± 0.02, respectively, for same sign and opposite sign K-D^* pairs. The simulation is modified accordingly and the remaining systematic uncertainty from this source becomes negligible;

(iv) *fake kaon candidate (mainly pions) (6%) or fake electrons (1%)*. Differences between data and MC on the evaluation of fake rates have been studied in *BABAR*. As this affects small components of the total peaking background rate, the effect of these differences has been neglected.

6. Fitting procedure and radiative events

To fit form-factor parameters we compare the number of expected events in each bin with the measured one after all corrections. In this approach it is always assumed that the q^2 variation of $f_+(q^2)$ is given exactly by the form-factor parameterization. This hypothesis is not correct, *a priori*, for radiative decays as $q^2 = (p_D - p_K)^2 = (p_e + p_\nu + p_\gamma)^2$ is not (perhaps) equal to the variable that enters in f_+ for such decays. PHOTOS is used to generate decays with additional photons and the modified pole ansatz is taken to parameterize the hadronic form factor in signal events. To quantify possible distortion of the fit we compare the fitted value of a form-factor parameter with the one obtained from a fit to the generated q^2 distribution (see Table IV).

Corresponding corrections, given in the second column of Table IV, have been applied and quoted uncertainties enter in the systematic uncertainty evaluation.

To evaluate the importance of corrections induced by radiative effects, we have compared also the fitted value of a parameter on q^2 distributions generated with and without using PHOTOS. Measured differences are given in the last column of Table IV. They have been applied to the values quoted in Table III for the different parameters. We measure also that radiative effects affect mainly the fraction of the decay spectrum in the first bin in Table II which has to be increased by 0.0012 to correct for this effect.

7. Control of the statistical accuracy in the SVD approach

Once the number of SV is fixed, one must verify that the statistical precision obtained for each binned unfolded value is correct and if biases generated by removing information are under control. These studies are done with toy simulations. One observes that the uncertainty obtained from a fit of the unfolded distribution is underestimated by a factor which depends on the statistics of simulated events and is ~1.06 in the present analysis. Pull distributions indicate also that the unfolded values, in each bin, have biases which are below 10% of the statistical uncertainty. Similar studies are done for the determination of form-factor parameters.

8. Summary of systematic errors

The systematic uncertainties for determining form-factor parameters are summarized in Table V.

The systematic error matrix for the ten unfolded values is computed by considering, in turn, each source of uncertainty and by measuring the variation, δ_i, of the corresponding unfolded value in each bin (i). The elements of this matrix are the sum, over all sources of systematic uncertainty, of the quantities $\delta_i \cdot \delta_j$. The total error matrix is evaluated as the sum of the matrices corresponding, respectively, to statistical and systematic uncertainties.

TABLE IV. Measured differences between the nominal and fitted values of parameters. Quoted uncertainties correspond to MC statistics. The last column gives the impact of the radiative effects on the form-factor measurements as predicted by PHOTOS.

Parameter	Measured difference (true-fitted)	Bias from radiation
$\delta(r_1)$ ($\times$ 0.01)	1.2 ± 13.0	−0.4 ± 2.7
$\delta(r_2)$	+1.7 ± 3.6	+1.9 ± 0.7
$\delta(\alpha_{\rm pole})$ ($\times$ 0.01)	−1.2 ± 1.4	−1.1 ± 0.3
$\delta(m_{\rm pole})$ (MeV/c^2)	+4.5 ± 6.3	+4.6 ± 1.4
$\delta(\alpha_I)$ ($\times$ 0.001 GeV^{-2})	−2.7 ± 3.1	−2.4 ± 0.7

TABLE V. Summary of systematic uncertainties on the fitted parameters.

Source	$\delta(m_{\rm pole})$ (MeV/c^2)	$\delta\alpha_{\rm pole}$ ($\times$ 0.01)	$\delta(\alpha_I)$ ($\times$ 0.001 GeV^{-2})	$\delta(r_1)$ ($\times$ 0.01)	$\delta(r_2)$
c-hadronization tuning	3.0	0.6	1.1	6.7	1.4
Reconstruction algorithm	7.8	1.6	3.1	6.5	0.2
Resolution on q^2	3.4	0.7	1.4	3.0	2.1
Particle ID	5.5	1.1	2.3	3.8	0.4
Background estimate	9.9	1.8	4.0	16.5	2.6
Fitting procedure	6.3	1.4	3.1	13.0	3.6
Total	15.8	3.1	6.6	23.5	5.1

B. Comparison with expectations and with other measurements

The summary of the fits to the normalized q^2 distributions are presented in Table III. As long as we allow the form-factor parameters to be free in the fit, the fitted distributions agree well with the data and it is not possible to reject any of the parameterizations.

However, if the form-factor parameters are constrained to specific predicted values, the agreement is not good. For the ISGW2 model, the predicted dependence of the form factor on q^2 disagrees with the data (see Table III) and the fitted value of the parameter α_I differs from the predicted value, $\alpha_I = 0.104$ GeV^{-2} by more than a factor two.

As observed by previous experiments, the simple pole model ansatz, with $m_{\rm pole} = m_{D_s^*} = 2.112$ GeV$/c^2$ does not reproduce the measurements. This means that the contribution from the continuum DK interaction cannot be neglected. If one introduces a second parameter $\delta_{\rm pole}$ to account for contributions from an effective pole at higher mass [see Eq. (10)] the two parameters are fully correlated and there is no unique solution, as illustrated in Fig. 8. The modified pole ansatz corresponds to $\delta_{\rm pole} = 0$.

In Table VI the fitted parameters for the simple pole ansatz and the modified pole [11] ansatz are compared for different experiments. The fitted pole masses are all well below the mass of the D_s^* meson. The results presented here are consistent within the stated uncertainties with earlier measurements. Except for the BELLE measurement, all other measurements appear to favor a value of $\alpha_{\rm pole}$ that is lower than the value predicted by lattice QCD, namely $\alpha_{\rm pole} = 0.50 \pm 0.04$.

TABLE VI. Fitted values for the parameters corresponding, respectively, to a pole mass and a modified pole mass model for the form-factor.

Experiment	$m_{\rm pole}$ (GeV/c^2)	$\alpha_{\rm pole}$
CLEO [4]	$1.89 \pm 0.05^{+0.04}_{-0.03}$	$0.36 \pm 0.10^{+0.03}_{-0.07}$
FOCUS [5]	$1.93 \pm 0.05 \pm 0.03$	$0.28 \pm 0.08 \pm 0.07$
BELLE [6]	$1.82 \pm 0.04 \pm 0.03$	$0.52 \pm 0.08 \pm 0.06$
This analysis	$1.884 \pm 0.012 \pm 0.016$	$0.38 \pm 0.02 \pm 0.03$

In Fig. 10, the dependence of the form factor on q^2 is presented. The data are compared to earlier measurements by the FOCUS experiment, as well as with predictions from lattice QCD calculations [19]. As stated above, the data favor a somewhat lower value for $\alpha_{\rm pole}$.

The data have also been mapped into the variable z. Figure 11 shows the product $P \times \Phi \times f_+$ as a function of z. By convention, this quantity is constrained to unity at $z = z_{\rm max}$, which corresponds to $q^2 = 0$. We perform a fit to a polynomial, $P \times \Phi \times f_+ \sim 1 + r_1 z + r_2 z^2$. The data are compatible with a linear dependence, which is fully consistent with the modified pole ansatz for $f_+(q^2)$, as illustrated in Fig. 11.

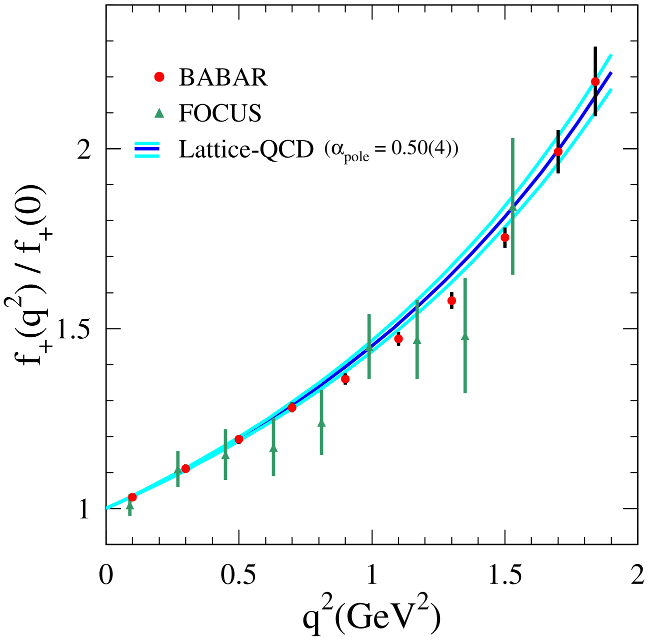

FIG. 10 (color online). Comparison of the measured variation of $f_+(q^2)/f_+(0)$ obtained in the present analysis and in the FOCUS experiment [5]. The band corresponds to lattice QCD [19] with the estimated uncertainty.

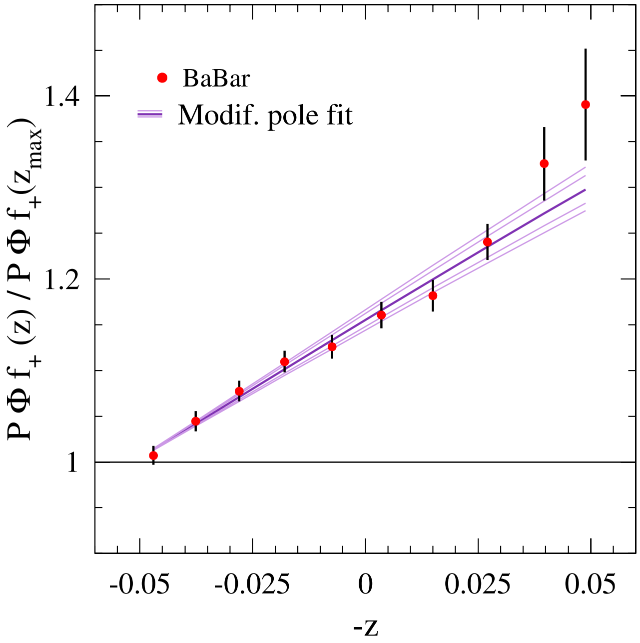

FIG. 11 (color online). Measured values for $P \times \Phi \times f_+(z)$, normalized to unity for $z = z_{\max} = 0.051$, are plotted versus $-z$. The straight lines represent the result for the modified pole ansatz, the fit in the center and the statistical and total uncertainty.

VI. BRANCHING FRACTION MEASUREMENT

The $D^0 \to K^- e^+ \nu_e$ branching fraction is measured relative to the reference decay channel, $D^0 \to K^- \pi^+$. Events with a radiated photon are included in the signal sample. Specifically, we compare the ratio of rates for the decay chains $D^{*+} \to D^0 \pi^+$, $D^0 \to K^- e^+ \nu_e(\gamma)$, and $D^0 \to K^- \pi^+(\gamma)$ in data and simulated events; this way, many systematic uncertainties cancel,

$$\begin{aligned} R_D &= \frac{\mathcal{B}(D^0 \to K^- e^+ \nu_e(\gamma))_{\text{data}}}{\mathcal{B}(D^0 \to K^- \pi^+(\gamma))_{\text{data}}} \\ &= \frac{\mathcal{B}(D^0 \to K^- e^+ \nu_e)_{\text{MC}}}{\mathcal{B}(D^0 \to K^- \pi^+)_{\text{MC}}} \times \frac{N(c\bar{c})_{Ke\nu}}{N(c\bar{c})_{K\pi}} \times \frac{\mathcal{L}(\text{data})_{K\pi}}{\mathcal{L}(\text{data})_{Ke\nu}} \\ &\quad \times \frac{N(D^0 \to K^- e^+ \nu_e)_{\text{data}}}{N(D^0 \to K^- e^+ \nu_e)_{\text{MC}}} \times \frac{N(D^0 \to K^- \pi^+)_{\text{MC}}}{N(D^0 \to K^- \pi^+)_{\text{data}}} \\ &\quad \times \frac{\epsilon(D^0 \to K^- e^+ \nu_e)_{\text{MC}}}{\epsilon(D^0 \to K^- e^+ \nu_e)_{\text{data}}} \times \frac{\epsilon(D^0 \to K^- \pi^+)_{\text{data}}}{\epsilon(D^0 \to K^- \pi^+)_{\text{MC}}} \end{aligned} \quad (15)$$

(to simplify these expressions, apart in the first fraction, the notation for radiated γ(s) has been omitted.)

The first line in this expression is the ratio of the branching fractions for the two channels used in the simulation:

$$\frac{\mathcal{B}(D^0 \to K^- e^+ \nu_e)_{\text{MC}}}{\mathcal{B}(D^0 \to K^- \pi^+)_{\text{MC}}} = \frac{0.0364}{0.0383}. \quad (16)$$

The second line is the ratio of the number of $c\bar{c}$ simulated events and the integrated luminosities for the two channels:

$$\frac{N(c\bar{c})_{Ke\nu}}{N(c\bar{c})_{K\pi}} \frac{\mathcal{L}(\text{data})_{K\pi}}{\mathcal{L}(\text{data})_{Ke\nu}} = \frac{117.0 \times 10^6}{117.3 \times 10^6} \times \frac{73.43 \text{ fb}^{-1}}{74.27 \text{ fb}^{-1}} \quad (17)$$

The third line corresponds to the ratios of measured numbers of signal events in data and in simulation, and the last line gives the ratios of the efficiencies to data and simulation.

A. Selection of candidate signal events

The selection of $D^0 \to K^- e^+ \nu_e$ candidates is explained in Secs. IV A and IV B. For the rate measurement, the constraint on the D^{*+} mass is not applied and also the momentum of the soft pion candidate is not included in the Fisher discriminant variable designed to suppress $B\bar{B}$ background. Since generic simulated signal events used in this measurement have been generated with the ISGW2 model, they have been weighted so that their q^2 distribution agrees with the measurement presented in this paper. Furthermore, we require for the Fisher discriminant $F_{B\bar{B}} > 0$ and restrict $\delta(m) < 0.16\ \text{GeV}/c^2$. After background subtraction, there remain 76283 ± 323 and 95302 ± 309 events in data and simulation, respectively. This gives

$$\frac{N(D^0 \to K^- e^+ \nu_e)_{\text{data}}}{N(D^0 \to K^- e^+ \nu_e)_{\text{MC}}} = 0.8004 \pm 0.0043. \quad (18)$$

To select $D^0 \to K^- \pi^+$ candidates, the same data samples are used (in practice the overlap between the two data sets is higher than 95%) and particles, in each event, are selected in the same way. The same selection criteria on the Fisher discriminant to suppress $B\bar{B}$-events, on the thrust axis direction and on other common variables are applied. Events are also analyzed in the same way, with two hemispheres defined from the thrust axis. In each hemisphere a D^0 candidate is reconstructed by combining a charged K with a pion of opposite sign. These tracks have to form a vertex and the $K\pi$ mass must be within the range $[1.77, 1.95]\ \text{GeV}/c^2$. Another charged pion of appropriate sign is added to form a D^{*+} candidate.

In addition, the following selection criteria are used:

(i) the fraction of the beam momentum, in the c.m. frame, taken by the D^* candidate must exceed 0.48 to remove contributions from $B\bar{B}$ events;
(ii) the measured D^0 mass must be in the range between 1.83 and 1.89 GeV/c^2. This requirement eliminates possible contributions from remaining $D^0 \to K^- K^+$ or $\pi^+ \pi^-$ decays [see Fig. 12(a)];
(iii) the vertex fits for the D^0 and D^* have to converge.

The $\delta(m)$ distribution for candidate events is shown in Fig. 12(c). The following components contribute to the D^{*+} signal [see Fig. 12(b)]:

(i) $D^0 \to K^- \pi^+$ with no extra photon;
(ii) $D^0 \to K^- \pi^+$ with at least one extra photon;
(iii) $D^0 \to K^- \pi^+(\gamma)$ where a π^+, mainly from the D^{*+}, decays into a muon.

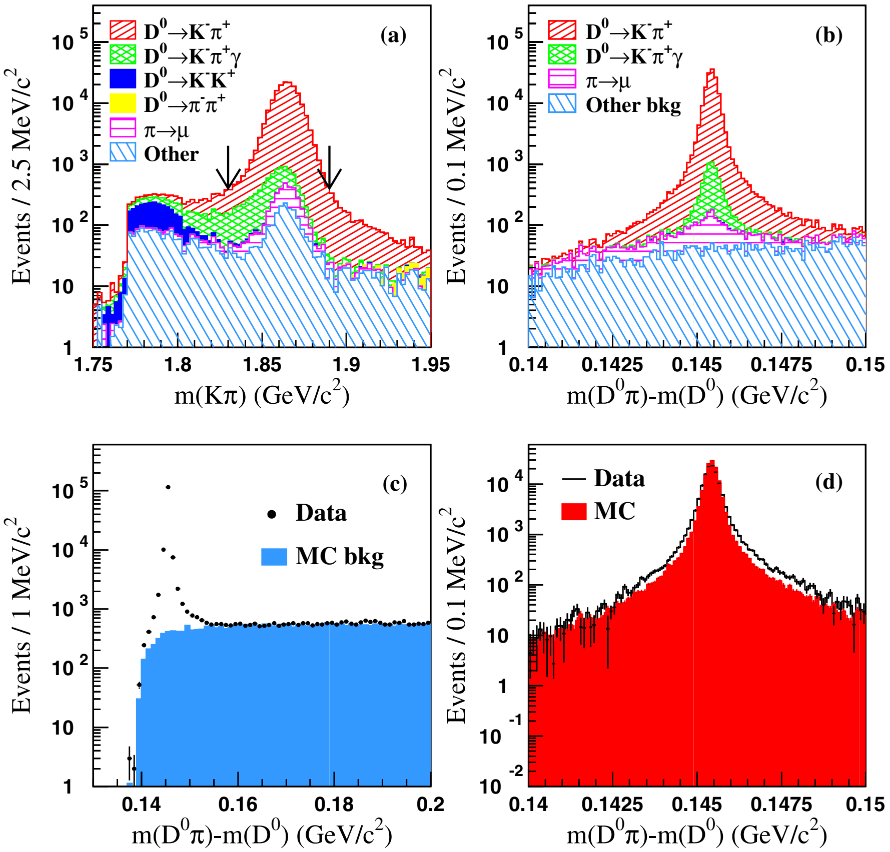

FIG. 12 (color online). Events selected for the reference channel $D^{*+} \to D^0\pi^+$, $D^0 \to K^-\pi^+$. (a) $K\pi$ mass distribution for events selected in the range $\delta(m) \in [0.143, 0.148]\ \mathrm{GeV}/c^2$. (b) $\delta(m)$ distribution for events selected in the range $m(K\pi) \in [1.83, 1.89]\ \mathrm{GeV}/c^2$. (c) same distribution as in (b), displayed on a larger mass range with the nonpeaking background indicated (shaded area). (d) $\delta(m)$ distribution after nonpeaking background subtraction, data (points with statistical errors) and simulated events (shaded histogram).

The $\delta(m)$ distribution corresponding to other event categories does not show a peaking component in the D^{*+} signal region. The total background level, is normalized to data using events in the $\delta(m)$ interval between 0.165 and $0.200\ \mathrm{GeV}/c^2$ [see Fig. 12(c)]. This global scaling factor is equal to 1.069 ± 0.011. After background subtraction, the $\delta(m)$ distributions obtained in data and simulation can be compared in Fig. 12(d). Since the D^{*+} signal is narrower in the simulation, we use a mass window such that this difference has a small effect on the measured number of D^{*+} events in data and in the simulation. There are $166\,960 \pm 409$ and $134\,537 \pm 374$ candidates selected in the interval $\delta(m) \in [0.142, 0.149]\ \mathrm{GeV}/c^2$ for simulated and data events, respectively. This means:

$$\frac{N(D^0 \to K^-\pi^+)_{\mathrm{MC}}}{N(D^0 \to K^-\pi^+)_{\mathrm{data}}} = 1.230 \pm 0.0046. \qquad (19)$$

B. Efficiency corrections

The impact of the selection requirement on the reconstructed $K\pi$ mass has been studied. The $K\pi$ mass distribution signal for simulated events (not including radiative photons) is compared with the corresponding distribution obtained with data after background subtraction. The background contributions are taken from the simulation. The fraction of D^0 candidates in the selected mass range (between 1.83 and $1.89\ \mathrm{GeV}/c^2$) is $(97.64 \pm 0.25)\%$ in MC and $(97.13 \pm 0.29)\%$ in data events. The ratio of efficiencies is equal to

$$\frac{\epsilon(D^0 \to K^-\pi^+)_{\mathrm{data}}}{\epsilon(D^0 \to K^-\pi^+)_{\mathrm{MC}}} = 0.9947 \pm 0.0039. \qquad (20)$$

Since $D^0 \to K^-e^+\nu_e$ events have been selected using a selection requirement on $\delta(m)$, we need to confirm that the distribution of this variable is similar in data and simulation. This is checked by comparing the distributions obtained with $D^0 \to K^-\pi^+\pi^0$ events analyzed as if they were semileptonic decays. The $\delta(m)$ distributions are compared in Fig. 13. Below $0.16\ \mathrm{GeV}/c^2$, there are $0.93552 \pm 0.000\,66$ of the D^{*+} candidates in the simulation and $0.93219 \pm 0.000\,78$ for data. The corresponding ratio of efficiencies (MC/data) is equal to 1.0036 ± 0.0010.

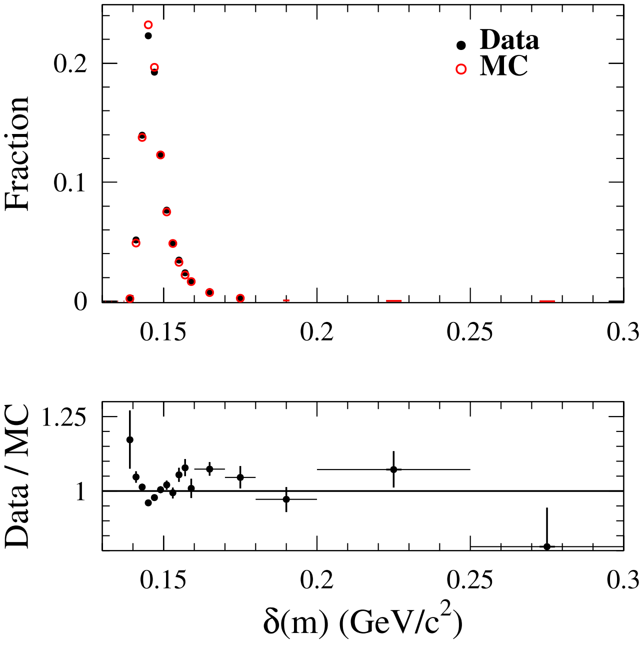

FIG. 13 (color online). $\delta(m)$ distribution for $D^0 \to K^- \pi^+ \pi^0$ events analyzed as if they were semileptonic decays. Distributions have been normalized to unity; note that the bin size is not uniform. The bottom plot shows the ratio of the two distributions above.

Using $D^0 \to K^- \pi^+ \pi^0$ events, we also measure the difference between the fraction of events retained after the mass-constrained fits. Namely, it is $0.980\,38 \pm 0.000\,37$ in the simulation compared to $0.97438 \pm 0.000\,49$ in data. The relative efficiency (MC/data) for this selection is 1.0062 ± 0.0006. Based on these two measured corrections the ratio of efficiencies are:

$$\frac{\epsilon(D^0 \to K^- e^+ \nu_e)_{\rm MC}}{\epsilon(D^0 \to K^- e^+ \nu_e)_{\rm data}} = 1.0098 \pm 0.0011. \qquad (21)$$

The quoted uncertainties, in this section, are of statistical origin and will be included in the statistical uncertainty on R_D. Other differences between the two analyzed channels are considered in the following section and contribute to systematic uncertainties.

C. Systematic uncertainties on R_D

A summary of the systematic uncertainties on R_D are given in Table VII. They originate from selection criteria which are different for the two channels. Some of these uncertainties are the same as those already considered for the determination of the q^2 variation of f_+.

1. Correlated systematic uncertainties

Systematic uncertainties on the decay rate coming from effects that contribute in the measurement of the q^2 dependence of $f_+(q^2)$ are evaluated in Sec. VA and the full covariance matrix for the measurements of the number of $D^0 \to K^- e^+ \nu_e$ signal events and the fraction of the decay spectrum fitted in each of the ten bins is determined. Among the sources of systematic uncertainties, listed in Table V, those corresponding to:

(i) the reconstruction algorithm,
(ii) the tuning of the resolution on q^2,
(iii) the corrections applied on electron identification, and
(iv) the background normalization

are taken as common sources. Corresponding relative uncertainties on R_D are given in Table VII.

TABLE VII. Summary of systematic uncertainties on the relative decay rate measurement.

Source	Relative variation
Reconstruction algorithm	±0.42%
Resolution on q^2	∼0
Electron ID	±0.56%
Background subtraction	±0.63%
Cut on Fisher variable	±0.76%
D^{*+} counting ($D^0 \to K^- \pi^+$)	±0.40%
Total	±1.27%

Other systematic uncertainties contributing to the form-factor measurement also affect the reference channel and so their effects on R_D cancel. They are related to the c-hadronization tuning and to the corrections applied on the kaon identification.

2. Selection requirement on the Fisher discriminant

The stability of the fraction of $D^0 \to K^- e^+ \nu_e$ events selected in data and in simulation as a function of the Fisher discriminant, F_{cc}, designed to suppress $c\bar{c}$ background has been examined. This is done by comparing the distributions of this variable measured in data and in simulation as given in Fig. 4 for two selected intervals in $\delta(m)$.

The value corresponding to $F_{cc} > 0$ and for events selected in the range $\delta(m) < 0.16$ GeV$/c^2$ is used as the central result and half the difference between the measurements corresponding to F_{cc} greater than -0.25 and $+0.25$ is taken as systematic uncertainty. This range corresponds to a relative change of 40% of the efficiency for signal events, and gives an uncertainty of ± 0.0061 on the ratio of data and simulated signal candidates given in Eq. (18).

3. D^{*+} counting in $D^0 \to K^- \pi^+$

D^{*+} candidates are selected in the range $\delta(m) \in [0.142, 0.149]$ GeV$/c^2$. From the simulation it is expected that the fraction of signal events outside this interval is equal to 1.4%. Even though the D^{*+} signal is slightly narrower in the simulation, there is not a large discrepancy in the tails. The fraction of signal events measured in the sidebands $\delta(m) \in [0.140, 0.142] \oplus [0.149, 0.150]$ GeV/c^2 is 0.4% and 0.5%, respectively, for simulation and data. An uncertainty of ± 0.004, corresponding to 30% uncertainty on the total fraction of events outside the selected $\delta(m)$ interval is assumed.

D. Decay rate measurement

Combining all measured fractions in Eq. (15), the measured relative decay rate is:

$$R_D = 0.9269 \pm 0.0072 \pm 0.0119. \tag{22}$$

Using the world average for the branching fraction $\mathcal{B}(D^0 \to K^- \pi^+) = (3.80 \pm 0.07)\%$ [1], gives $\mathcal{B}(D^0 \to K^- e^+ \nu_e(\gamma)) = (3.522 \pm 0.027 \pm 0.045 \pm 0.065)\%$, where the last quoted uncertainty corresponds to the accuracy on $\mathcal{B}(D^0 \to K^- \pi^+)$.

VII. SUMMARY

The decay rate distribution for the channel $D^0 \to K^- e^+ \nu_e(\gamma)$ has been measured in ten bins of q^2 in Table II. Several theoretical expectations for the variation of this form factor with q^2 have been considered and values for the corresponding parameters have been obtained (see Table III). The q^2 variation of the form factor can be parameterized with a single parameter using different expressions. The ISGW2 model with expected values for the parameters is excluded, as is the pole mass parameterization with $m_{\rm pole} = m_{D_s^*}$.

The value of the decay branching fraction has been also measured independent of a model in Section VI D.

Combining these measurements and integrating Eq. (2), the value of the hadronic form factor is obtained:

$$f_+(0) = \frac{1}{|V_{cs}|}\sqrt{\frac{24\pi^3}{G_F^2}\frac{\mathcal{B}}{\tau_{D^0} I}}, \tag{23}$$

where $\mathcal{B}$ is the measured $D^0 \to K^- e^+ \nu_e$ branching fraction, $\tau_{D^0} = (410.1 \pm 1.5) \times 10^{-15}$ s [1] is the D^0 lifetime and $I = \int_0^{q^2_{\rm max}} |\vec{p}_K(q^2)|^3 |f_+(q^2)/f_+(0)|^2 dq^2$. To account for the variation of the form factor within one bin, and, in particular, to extrapolate the result at $q^2 = 0$, the pole mass and the modified pole ansatze have been used; the corresponding values obtained for $f_+(0)$ differ by 0.002. Taking the average between these two values and including their difference in the systematic uncertainty, this gives

$$f_+(0) = 0.727 \pm 0.007 \pm 0.005 \pm 0.007, \tag{24}$$

where the last quoted uncertainty corresponds to the accuracy on $\mathcal{B}(D^0 \to K^- \pi^+)$, τ_{D^0} and $|V_{cs}|$. It agrees with expectations and, in particular, with LQCD computations [19]. Using the z expansion of Eq. (6) and assuming that $m_c = 1.2$ GeV/c^2 to evaluate χ_V from Eq. (8), we find $a_0 = (2.98 \pm 0.01 \pm 0.03 \pm 0.03) \times 10^{-2}$.

The high accuracy of the present measurement will be a reference test for improved lattice determinations of the q^2 variation of f_+.

ACKNOWLEDGMENTS

The authors wish to thank R. J. Hill, D. Becirevic, C. Bernard, Ph. Boucaud, S. Descotes-Genon, L. Lellouch, J.-P. Leroy, A. Le Yaouanc, and O. Pène for their help with the theoretical interpretation of these results. We are grateful for the extraordinary contributions of our PEP-II colleagues in achieving the excellent luminosity and machine conditions that have made this work possible. The success of this project also relies critically on the expertise and dedication of the computing organizations that support *BABAR*. The collaborating institutions wish to thank SLAC for its support and the kind hospitality extended to them. This work is supported by the US Department of Energy and National Science Foundation, the Natural Sciences and Engineering Research Council (Canada), the Institute of High Energy Physics (China), the Commissariat à l'Energie Atomique and Institut National de Physique Nucléaire et de Physique des Particules (France), the Bundesministerium für Bildung und Forschung and Deutsche Forschungsgemeinschaft (Germany), the Istituto Nazionale di Fisica Nucleare (Italy), the Foundation for Fundamental Research on Matter (The Netherlands), the Research Council of Norway, the Ministry of Science and Technology of the Russian Federation, Ministerio de Educación y Ciencia (Spain), and the Particle Physics and Astronomy Research Council (United Kingdom). Individuals have received support from the Marie-Curie IEF program (European Union) and the A. P. Sloan Foundation.

---

[1] W.-M. Yao *et al.*, J. Phys. G **33**, 1 (2006).
[2] Charge conjugate states are implied throughout this analysis.
[3] J. G. Koerner and G. A. Schuler, Z. Phys. C **46**, 93 (1990); F. J. Gilman and R. L. Singleton, Jr., Phys. Rev. D **41**, 142 (1990).
[4] G. S. Huang *et al.* (CLEO Cllaboration), Phys. Rev. Lett. **94**, 011802 (2005).
[5] J. M. Link *et al.* (FOCUS Collaboration), Phys. Lett. B **607**, 233 (2005).
[6] L. Widhalm *et al.* (BELLE Collaboration), Phys. Rev. Lett. **97**, 061804 (2006).
[7] T. Becher and R. J. Hill, Phys. Lett. B **633**, 61 (2006).
[8] C. G. Boyd and M. J. Savage, Phys. Rev. D **56**, 303 (1997),

and references therein.
[9] C. G. Boyd, B. Grinstein, and R. F. Lebed, Nucl. Phys. **B461**, 493 (1996).
[10] The variation of χ_V with $u = m_s/m_c$ is small, since $\chi_V(0.33) = 1.02 \times \chi_V(0)$.
[11] D. Becirevic and A. B. Kaidalov, Phys. Lett. B **478**, 417 (2000).
[12] M. Wirbel, B. Stech, and M. Bauer, Z. Phys. C **29**, 637 (1985); J. G. Körner and G. A. Schuler, Z. Phys. C **38**, 511 (1988); **41**, 690(E) (1988); M. Bauer and M. Wirbel, Z. Phys. C **42**, 671 (1989); J. G. Körner, K. Schilcher, M. Wirbel, and Y. L. Wu, Z. Phys. C **48**, 663 (1990); W. Jaus, Phys. Rev. D **41**, 3394 (1990); **53**, 1349 (1996); R. Aleksan, A. Le Yaouanc, L. Oliver, O. Pène, and J. C. Raynal, Phys. Rev. D **51**, 6235 (1995); I. L. Grach, I. M. Narodetskii, and S. Simula, Phys. Lett. B **385**, 317 (1996); H. M. Choi and C. R. Ji, Phys. Lett. B **460**, 461 (1999); D. Melikhov and B. Stech, Phys. Rev. D **62**, 014006 (2000); G. Amoros, S. Noguera, and J. Portoles, Eur. Phys. J. C **27**, 243 (2003); W. Y. Wang, Y. L. Wu, and M. Zhong, Phys. Rev. D **67**, 014024 (2003); S. Fajfer and J. Kamenik, Phys. Rev. D **71**, 014020 (2005).
[13] N. Isgur, D. Scora, B. Grinstein, and M. B. Wise, Phys. Rev. D **39**, 799 (1989).
[14] D. Scora and N. Isgur, Phys. Rev. D **52**, 2783 (1995).
[15] T. M. Aliev, V. L. Eletsky, and Ya. I. Kogan, Sov. J. Nucl. Phys. **40**, 527 (1984); P. Ball, V. M. Braun, and H. G. Dosch, Phys. Rev. D **44**, 3567 (1991).
[16] A. Khodjamirian, R. Rückl, S. Weinzierl, C. W. Winhart, and O. Yakovlev, Phys. Rev. D **62**, 114002 (2000).
[17] J. M. Flynn and C. T. Sachrajda, in *Heavy Flavours*, edited by A. J. Buras and M. Linder (World Scientific, Singapore, 1998), 2nd ed. Published in Adv. Ser. Dir. High Energy Phys. **15**, 402 (1998).
[18] A. Abada *et al.*, Nucl. Phys. **B619**, 565 (2001).
[19] C. Aubin *et al.*, Phys. Rev. Lett. **94**, 011601 (2005).
[20] B. Aubert *et al.* (*BABAR* Collaboration), Nucl. Instrum. Methods Phys. Res., Sect. A **479**, 1 (2002).
[21] B. Aubert *et al.* (*BABAR* Collaboration), Phys. Rev. D **66**, 032003 (2002).
[22] S. Agostinelli *et al.*, Nucl. Instrum. Methods A **506**, 250 (2003).
[23] T. Sjöstrand, Comput. Phys. Commun. **82**, 74 (1994).
[24] E. Barberio and Z. Was, Comput. Phys. Commun. **79**, 291 (1994).
[25] J. M. Link *et al.* (FOCUS Collaboration), Phys. Lett. B **544**, 89 (2002).
[26] G. C. Fox and S. Wolfram, Phys. Rev. Lett. **41**, 1581 (1978).
[27] A. Hocker and V. Kartvelishvili, Nucl. Instrum. Methods Phys. Res., Sect. A **372**, 469 (1996).
[28] M. Artuso *et al.* (CLEO Collaboration), Phys. Rev. D **70**, 112001 (2004).